Duality and Unified Analysis of Discrete Approximations in Structural Dynamics and Wave Propagation: Comparison of *p*-method Finite Elements with *k*-method NURBS

T.J.R. Hughes [a,*], A. Reali [b,d,e], G. Sangalli [c,e]

[a] *Institute for Computational Engineering and Sciences, University of Texas at Austin*

[b] *Dipartimento di Meccanica Strutturale, Università degli Studi di Pavia*

[c] *Dipartimento di Matematica, Università degli Studi di Pavia*

[d] *European Centre for Training and Research in Earthquake Engineering, Pavia*

[e] *Istituto di Matematica Applicata e Tecnologie Informatiche del CNR, Pavia*

"Comparisons are Odious", *De Laudibus Legum Angliae*, John Fortescue, c. 1394–1476.

Abstract

We study the discretization behavior of classical finite element and NURBS approximations on problems of structural vibrations and wave propagation. We find that, on the basis of equal numbers of degrees-of-freedom and bandwidth, NURBS have superior approximation properties. In fact, we observe that the high mode behavior of classical finite elements is divergent with the order of approximation, a surprisingly negative result. On the other hand, NURBS offer almost spectral approximation properties, and all modes converge with increasing order of approximation.

Key words: Structural vibrations, Wave propagation, Eigenvalue problems, Dispersion Analysis, Finite elements, NURBS, B-splines, Acoustic branches, Optical branches, Frequency errors, Amplitude spectra, Frequency response spectra, Evanescent waves, Stopping bands

* Corresponding author.
Address: 201 East 24th Street, ACES 5.430A, 1 University Station, C0200, Austin, TX 78712-0027, U.S.A.
Phone: +1 512 232 7775. Fax: +1 512 232 7508
E-mail: hughes@ices.utexas.edu

Contents

1 Introduction

Isogeometric Analysis was introduced by Hughes, Cottrell and Bazilevs [15] in an effort to improve upon shortcomings of finite element analysis in the areas of geometric precision, ease of mesh refinement, and integration with Computer Aided Design (CAD). Engineering investigations of performance in vibration calculations showed very good behavior, Cottrell *et al.* [7], as did mathematical studies of convergence under mesh refinement, Bazilevs *et al.* [2]. Nevertheless, the approximability of isogeometric analysis compared with classical finite element analysis has not been thoroughly investigated. It is the purpose of this paper to initiate such a comparison.

To a certain degree, one might say that isogeometric analysis subsumes finite element analysis, in that standard element basis functions can be generated from B-splines and NURBS (non-uniform rational B-splines), the main technologies used thus far in the instantiation of isogeometric analysis. However, isogeometric analysis offers more, in particular, the possibility of developing smoother basis functions, at least throughout patches (i.e., subdomains), and in many cases globally. Isogeometric analysis emanates from constructs used in design, computer graphics, animation, and visualization, and it is often the case that smoothness is of utmost importance. For example, rendering of reflective objects requires essentially C^2-continuity in order not to exhibit spurious reflections. In recent years, a number of computer graphics techniques have been developed to address this issue. It is interesting to note that difficulties in developing smooth basis functions (i.e., C^1-continuity and higher) in the early years of finite elements usually led to reformulation of problems so that C^0-elements could be utilized, a classical illustration being the virtual abandonment of Poisson-Kirchhoff plate theory, which leads to fourth-order biharmonic problems, in favor of Reissner-Mindlin theory, which leads to second-order differential equations. Times have changed and it is now possible to construct complex models utilizing functions smoother than C^0. This may open a door to simpler formulations of problems involving higher-order differential operators (see, e.g., Gomez *et al.* [11]). Another possibility is that smoother functions might produce better approximations of derivatives than C^0 continuous finite elements in second-order problems. For example, stresses are generally the most important quantities in structural analysis, and they are usually smooth almost everywhere. Standard finite elements require smoothing and post-processing of stresses. This might be avoided through the use of smooth basis functions.

In this paper we initiate the investigation of smooth basis functions generated by isogeometric analysis and compare them with standard C^0 finite elements. The problems used as a basis of comparison emanate from structural dynamics and wave propagation, in particular the eigenvalue problem of free vibration, and the Helmholtz equation of time harmonic wave propagation arising in acoustics and electromagnetics. We use discrete Fourier techniques (see Richtmyer and Morton

[20]) to analyze the difference equations. In the case of the eigenvalue problem, we work with a finite domain and homogeneous Dirichlet boundary conditions, and for the Helmholtz equation we perform dispersion analysis on infinite domains, and consider a boundary-value problem on a finite domain.

The basis of comparison used throughout this paper is the number of degrees of freedom in the discrete model, which turns out to be equivalent to the bandwidth of the corresponding matrix problem. There is some precedent for this basis of comparison, namely, it was used by Kwok, Moser and Jiménez [17] in studies of B-splines, finite element, and collocation methods for advective and diffusive processes and they presented their rationale for selecting it. Nevertheless, one can still take issue with it, primarily, in our opinion, because it leads to significantly different numbers of quadrature points for smooth and C^0 basis functions. However, it may be said that, for the smooth case, optimal rules are not yet known and once they are, a more valid comparison of cost will be able to be made. In the meantime, we will use the number of degrees-of-freedom as a basis for comparison, but recognize that the issue is more complex.

In Section 2 we briefly review the problems under consideration. In Section 3 we recall the basis of isogeometric analysis, B-splines and NURBS. We describe the different geometric constructions which lead to linear and nonlinear parameterizations of the problem domain. This has important consequences in vibration analysis (see [7]). In Section 4 we begin our investigation in the context of one-dimensional problems. We calculate the discrete spectrum of the eigenproblem, and the dispersion properties of the discrete approximation to the Helmholtz problem using complex wave-number analysis [22]. After presenting the details for linear elements, we state a "duality principle", which enables us to map results of spectral analysis to dispersion analysis, and vice versa. Throughout the paper we invoke the duality principle to simplify derivations. Nevertheless, there are subtle differences between spectrum and dispersion analysis that need to be noted, namely, the possible existence of "outlier frequencies" [7] in spectrum analysis, and the existence of complex wave-numbers leading to spurious evanescent waves in dispersion analysis. These phenomena occur for higher-order discretizations and so we investigate quadratics in some detail, and sketch what happens in cubic and higher-order cases. We calculate the "stopping bands" for classical finite elements, first identified by Thompson and Pinsky [22], and show that B-splines/NURBS do not engender stopping bands. However, they produce spurious roots corresponding to evanescent waves. These are strongly attenuated and do not seem to show themselves in numerical calculations. We then proceed in Section 5 to a two-dimensional model problem that we analyze with bilinear elements. This problem gives us the opportunity to explain the oscillations in frequency errors produced in numerical studies. Based on results in Sections 3 and 4 we are able to confidently use numerics to calculate invariant analytical spectra for classical p-method finite elements and NURBS. This comparison is quite startling. The higher-order p-elements give rise to so-called "optical branches" to spectra, which have no approximation prop-

erties. It is well known that the upper part of discrete frequency spectra are very inaccurate, but what seems to be a completely new observation is the errors *diverge* with p. On the other hand there are no optical modes with NURBS (at least when an appropriate "nonlinear" parameterization of the geometry is used [7]) and the spectral errors *converge* with p. The results are strikingly different (see Figure 28) and seem to register a significant advantage for NURBS. We conjecture that these results may at least partially explain why classical higher-order finite elements have not been widely adopted in problems for which the upper part of the discrete spectrum participates in a significant way, such as, for example, impact problems and turbulence. We also examine eigenvectors in one dimension and two-dimensional spectra for higher-order approximations. This is followed by studies of frequency response spectra and wave propagation in a one-dimensional rod. In all cases, we find NURBS outperform standard finite elements. Our last study is an initiatory one into the effects of reduced numerical quadrature. We find that reducing quadrature, below exact, for p-method finite elements, has deleterious consequences. Now, not only spectra diverge with p, but for a fixed p, with only one point less than for the exact rule, they diverge with mesh refinement (i.e., h-refinement). The situation is much worse than for the exactly integrated case, which is certainly not good. It is also an indication that the Gauss rules are indeed optimal, as fewer points are disastrous. On the other hand, reducing quadrature for NURBS does not have significant effect. Roughly speaking, the Gauss rule with approximately half as many Gauss points as required for exact integration provides very acceptable results with no significant degradation. This indicates that the Gauss rules are far from optimal for NURBS. In fact, it is conceptually clear that the Gauss rules are not the answer because they do not acknowledge in any way the precise order of continuity at knots. So, at present, application of the Gauss rules between knots is simple and effective, but clearly very inefficient. We anticipate that optimal rules will eventually be developed for NURBS and, at that time, we will be able to make more equitable comparisons of cost. We draw conclusions in Section 7.

2 Structural vibrations and wave propagation

In this section we briefly recall the main equations of structural vibrations and of wave propagation; for elaboration, see Chopra [4], Clough and Penzien [5], and Hughes [14] for structural vibrations; Thompson and Pinsky [23], and Thompson [24] for wave propagation (note that in [23, 24] particular emphasis is on acoustics).

Given a linear (∞-dimensional) structural system, the undamped, unforced equations of motion, which govern free vibrations, are

$$\mathcal{M}\frac{\mathrm{d}^2\mathbf{u}}{\mathrm{d}t^2} + \mathcal{K}\mathbf{u} = \mathbf{0}, \tag{1}$$

where $\mathcal{M}$ and $\mathcal{K}$ are, respectively, the mass and stiffness operators, and $\mathbf{u} = \mathbf{u}(t, \mathbf{x})$ is the displacement.

The n^{th} normal mode $\boldsymbol{\phi}_n$ and its frequency ω_n are obtained from the following eigenvalue problem

$$\mathcal{K}\boldsymbol{\phi}_n = \omega_n^2 \mathcal{M}\boldsymbol{\phi}_n.$$

We remark that the normal modes form a basis in space.

Then, we can separate variables as

$$\mathbf{u}(t, \mathbf{x}) = \sum_n \hat{u}_n(t)\boldsymbol{\phi}_n(\mathbf{x}),$$

and, using equation (1), obtain

$$\frac{\mathrm{d}^2\hat{u}_n(t)}{\mathrm{d}t^2} + \omega_n^2\hat{u}_n(t) = 0.$$

Each mode coefficient $\hat{u}_n$ oscillates at a frequency ω_n, and we can write

$$\hat{u}_n = C_- e^{-\mathrm{i}\omega_n t} + C_+ e^{\mathrm{i}\omega_n t}.$$

After discretization, the following discrete equations of motion are obtained

$$\mathbf{M}\frac{\mathrm{d}^2\mathbf{u}^h}{\mathrm{d}t^2} + \mathbf{K}\mathbf{u}^h = \mathbf{0}, \tag{2}$$

where $\mathbf{M}$ and $\mathbf{K}$ are, respectively, the finite-dimensional consistent mass and stiffness matrices, and $\mathbf{u}^h = \mathbf{u}^h(t, \mathbf{x})$ is the discrete displacement vector.

Analogously to the continuum case, the discrete normal modes $\boldsymbol{\phi}_n^h$ and the frequencies ω_n^h are obtained from the eigenproblem

$$\mathbf{K}\boldsymbol{\phi}_n^h = (\omega_n^h)^2\mathbf{M}\boldsymbol{\phi}_n^h, \tag{3}$$

and separating variables we get

$$\mathbf{u}^h(t, \mathbf{x}) = \sum_n \hat{u}_n^h(t)\boldsymbol{\phi}_n^h(\mathbf{x}),$$

with $\hat{u}_n^h$ oscillating at a frequency ω_n^h, that is,

$$\hat{u}_n^h = C_- e^{-\mathrm{i}\omega_n^h t} + C_+ e^{\mathrm{i}\omega_n^h t}.$$

The n^{th} discrete normal mode $\boldsymbol{\phi}_n^h$ is an approximation of the n^{th} exact normal mode $\boldsymbol{\phi}_n$, for $n = 1, \ldots, N$, being N the total number of degrees-of-freedom.

The corresponding discrete and exact frequencies are of course different (see, e.g., Figure 1).

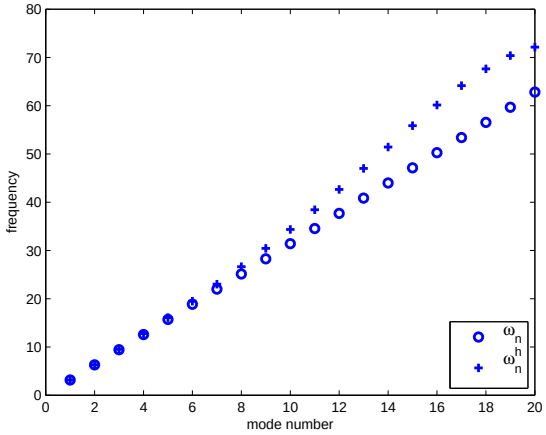

Fig. 1. Exact and discrete natural frequencies for the one-dimensional model problem of free vibration of an elastic rod with homogeneous Dirichlet boundary conditions. The discrete method is based on linear finite elements.

A fundamental question is, how close are the discrete frequencies to the continuous ones? In other words, how well does the discrete spectrum approximate the exact spectrum?

2.2 Wave propagation: the Helmholtz equation

The classical equation governing wave propagation is

$$\nabla^2 u - \frac{1}{c^2}\frac{\mathrm{d}^2 u}{\mathrm{d}t^2} = 0, \tag{4}$$

where c is the wave propagation speed. Particular solutions of (4) are plane waves of frequency ω traveling in the direction $\mathbf{n}$ at a speed c, which can be expressed as the time-harmonic wave train

$$u(\mathbf{x}, t) = Re(Ae^{\mathrm{i}(k\mathbf{n}\cdot\mathbf{x}-\omega t)}), \tag{5}$$

where $k = \omega/c$ is the wave-number, ω is the angular frequency, and A is a complex number. The wavelength (with units of length) is defined by $\lambda = 2\pi/k$, while the dual measure of period (with units of time) is defined by $T = 2\pi/\omega$.

Assuming time-harmonic solutions, that is, with abuse of notation, $u(t, \mathbf{x}) = e^{\mathrm{i}\omega t}u(\mathbf{x})$, the linear wave equation (4) reduces to the Helmholtz equation

$$\nabla^2 u + k^2 u = 0, \tag{6}$$

whose solutions in $\mathbb{R}^n$ are linear combinations of plane waves in space $u(\mathbf{x}) = e^{\mathrm{i}k\mathbf{n}\cdot\mathbf{x}}$. After discretization, equation (6) gives rise to

$$(\mathbf{K} - k^2\mathbf{M})\mathbf{u}^h = \mathbf{0}. \tag{7}$$

The numerical solution of the above equation is a linear combination of plane waves having numerical wave-number k^h, where, in general, $k^h \neq k$.

Thus, discrete and exact waves have different wavelengths, $2\pi/k^h$ and $2\pi/k$ (see Figure 2).

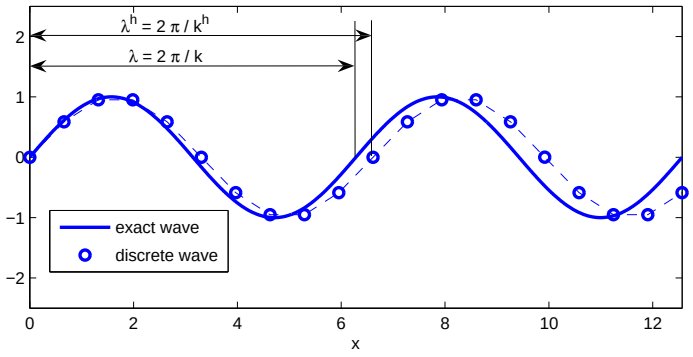

Fig. 2. Different exact and numerical wave-numbers produce waves with different wavelengths.

The fundamental issue, which is addressed by dispersion analysis, is to determine the dispersion of a numerical method, that is, how close the discrete wave-number k^h is to its continuous counterpart k.

3 NURBS-based isogeometric analysis

Non-Uniform Rational B-splines (NURBS) are a standard tool for describing and modeling curves and surfaces in computer aided design and computer graphics (see Piegl and Tiller [18] and Rogers [21] for an extensive description of these functions and their properties). In this work, we use NURBS as an analysis tool, which is referred to as "isogeometric analysis" by Hughes *et al.* [15]. The aim of

this section is to present a brief overview of features and properties of NURBS-based isogeometric analysis for 1D and 2D problems. We will utilize NURBS in our study of the problems introduced in the previous sections. The section starts with a short description of B-splines and NURBS.

3.1 B-splines and NURBS

B-splines in the plane are piecewise polynomial curves composed of linear combinations of B-spline basis functions. The coefficients are points in the plane, referred to as *control points*.

A *knot vector* is a set of non-decreasing real numbers representing coordinates in the parametric space of the curve

$$\{\xi_1 = 0, ..., \xi_{n+p+1} = 1\}, \tag{8}$$

where p is the order of the B-spline and n is the number of basis functions (and control points) necessary to describe it. The interval $[\xi_1, \xi_{n+p+1}]$ is called a *patch*. A knot vector is said to be *uniform* if its knots are uniformly-spaced and *non-uniform* otherwise. Moreover, a knot vector is said to be *open* if its first and last knots are repeated $p + 1$ times. In what follows, we always employ open knot vectors. Basis functions formed from open knot vectors are interpolatory at the ends of the parametric interval $[0, 1]$ but are not, in general, interpolatory at interior knots.

Given a knot vector, univariate B-spline basis functions are defined recursively starting with $p = 0$ (piecewise constants)

$$N_{i,0}(\xi) = \begin{cases} 1 \text{ if } \xi_i \leq \xi < \xi_{i+1} \\ 0 \text{ otherwise.} \end{cases} \tag{9}$$

For $p > 1$:

$$N_{i,p}(\xi) = \frac{\xi - \xi_i}{\xi_{i+p} - \xi_i} N_{i,p-1}(\xi) + \frac{\xi_{i+p+1} - \xi}{\xi_{i+p+1} - \xi_{i+1}} N_{i+1,p-1}(\xi). \tag{10}$$

In Figure 3 we present an example consisting of $n = 9$ cubic basis functions generated from the open knot vector $\{0, 0, 0, 0, 1/6, 1/3, 1/2, 2/3, 5/6, 1, 1, 1, 1\}$.

If internal knots are not repeated, B-spline basis functions are C^{p-1}-continuous. If a knot has multiplicity k, the basis is C^{p-k}-continuous at that knot. In particular, when a knot has multiplicity p, the basis is C^0 and interpolates the control point at that location.

By means of tensor products, a B-spline region can be constructed starting from knot vectors $\{\xi_1 = 0, ..., \xi_{n+p+1} = 1\}$ and $\{\eta_1 = 0, ..., \eta_{m+q+1} = 1\}$, and an $n \times m$

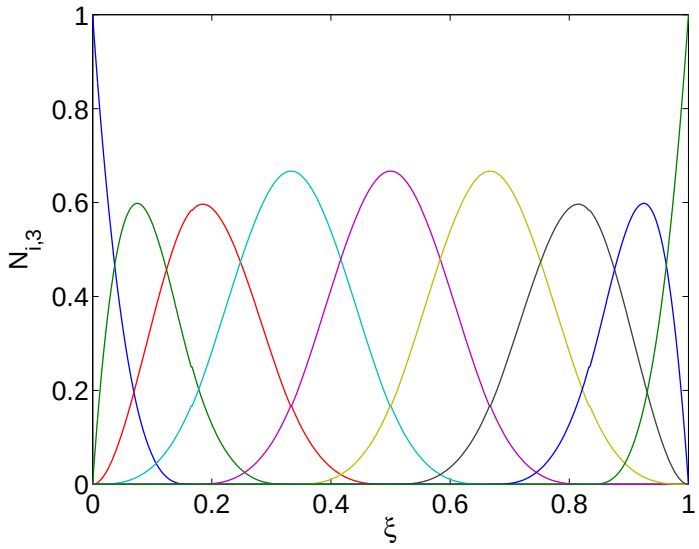

Fig. 3. Cubic basis functions formed from the open knot vector $\{0, 0, 0, 0, 1/6, 1/3, 1/2, 2/3, 5/6, 1, 1, 1, 1\}$.

net of control points $\mathbf{B}_{i,j}$. Two-dimensional basis functions $N_{i,p}$ and $M_{j,q}$ (with $i = 1, ..., n$ and $j = 1, ..., m$) of order p and q, respectively, are defined from the knot vectors, and the B-spline region is the image of the map $\mathbf{S} : [0, 1] \times [0, 1] \to \overline{\Omega}$ given by

$$\mathbf{S}(\xi, \eta) = \sum_{i=1}^{n} \sum_{j=1}^{m} N_{i,p}(\xi) M_{j,q}(\eta) \mathbf{B}_{i,j}. \tag{11}$$

The two-dimensional parametric space is the domain $[0, 1] \times [0, 1]$. Observe that the two knot vectors $\{\xi_1 = 0, ..., \xi_{n+p+1} = 1\}$ and $\{\eta_1 = 0, ..., \eta_{m+q+1} = 1\}$ generate in a natural way a mesh of rectangular elements in the parametric space.

A rational B-spline in $\mathbb{R}^2$ is the projection onto two-dimensional physical space of a polynomial B-spline defined in three-dimensional homogeneous coordinate space. For a complete discussion of these space projections, see [6, 10] and references therein. In this way, a great variety of geometrical entities can be constructed and, in particular, all conic sections in physical space can be obtained exactly. The projective transformation of a B-spline curve yields a rational polynomial curve. Note that when we refer to the "order" of a NURBS curve, we mean the order of the polynomial curve from which the rational curve was generated.

To obtain a NURBS curve in $\mathbb{R}^2$, we start from a set $\mathbf{B}_i^w \in \mathbb{R}^3$ ($i = 1, ..., n$) of control points ("projective points") for a B-spline curve in $\mathbb{R}^3$ with knot vector Ξ. Then the control points for the NURBS curve are

$$(\mathbf{B}_i)_j = \frac{(\mathbf{B}_i^w)_j}{w_i}, \; j = 1, 2 \tag{12}$$

where $(\mathbf{B}_i)_j$ is the j^{th} component of the vector $\mathbf{B}_i$ and $w_i = (\mathbf{B}_i^w)_3$ is referred to as

the i^{th} *weight*. The NURBS basis functions of order p are then defined as

$$R_i^p(\xi) = \frac{N_{i,p}(\xi) w_i}{\sum_{\hat{i}=1}^{n} N_{\hat{i},p}(\xi) w_{\hat{i}}}. \tag{13}$$

The NURBS curve is defined by

$$\mathbf{C}(\xi) = \sum_{i=1}^{n} R_i^p(\xi) \mathbf{B}_i. \tag{14}$$

Analogously to B-splines, NURBS basis functions on the two-dimensional parametric space $[0,1] \times [0,1]$ are defined as

$$R_{i,j}^{p,q}(\xi,\eta) = \frac{N_{i,p}(\xi) M_{j,q}(\eta) w_{i,j}}{\sum_{\hat{i}=1}^{n} \sum_{\hat{j}=1}^{m} N_{\hat{i},p}(\xi) M_{\hat{j},q}(\eta) w_{\hat{i},\hat{j}}}, \tag{15}$$

where $w_{i,j} = (\mathbf{B}_{i,j}^w)_3$. Observe that the continuity and support of NURBS basis functions are the same as for B-splines.

NURBS regions, similarly to B-spline regions, are defined in terms of the basis functions (15). In particular we assume from now on that the physical domain Ω is a NURBS region associated with the $n \times m$ net of control points $\mathbf{B}_{i,j}$, and we introduce the geometrical map $\mathbf{F} : [0,1] \times [0,1] \to \overline{\Omega}$ given by

$$\mathbf{F}(\xi,\eta) = \sum_{i=1}^{n} \sum_{j=1}^{m} R_{i,j}^{p,q}(\xi,\eta) \mathbf{B}_{i,j}. \tag{16}$$

3.2 Isogeometric Analysis

The image of the elements in the parametric space are elements in the physical space. The physical mesh is therefore

$$\mathcal{T}_h = \{\mathbf{F}((\xi_i, \xi_{i+1}) \times (\eta_j, \eta_{j+1})), \text{ with } i = 1, \ldots, n+p,\ j = 1, \ldots, m+q\}. \tag{17}$$

We denote by h the mesh-size, that is, the maximum diameter of the elements of $\mathcal{T}_h$.

Following the isoparametric approach, the space of NURBS functions on Ω is defined as the span of the *push-forward* of the basis functions (15)

$$\mathcal{V}_h = \text{span}\{R_{i,j}^{p,q} \circ \mathbf{F}^{-1}\}_{i=1,\ldots,n; j=1,\ldots,m}. \tag{18}$$

3.2.1 Main features

In the following we present a summary of the main features of isogeometric analysis. The interested reader may find more details and applications in [2, 7, 8, 15, 19].

- A mesh for a NURBS patch is defined by the product of knot vectors.
- Knot spans subdivide the domain into "elements".
- The support of each basis function consists of a small number of elements.
- The control points associated with the basis functions define the geometry.
- The isoparametric concept is invoked, that is, the unknown variables are represented in terms of the basis functions which define the geometry. The coefficients of the basis functions are the degrees-of-freedom, or *control variables*.
- Three different mesh refinement strategies are possible: analogues of classical *h*-refinement (by knot insertion) and *p*-refinement (by order elevation of the basis functions), and a new possibility referred to as *k*-refinement, which increases smoothness in addition to order.
- The element arrays constructed from isoparametric NURBS can be assembled into global arrays in the same way as finite elements (see Hughes [14], chapter 2).
- Dirichlet boundary conditions are applied to the control variables, in the same way as in finite elements. Neumann boundary conditions are satisfied naturally as in standard finite element formulations (see Hughes [14], chapters 1 and 2).

Finally, it is important to remark that in structural analysis NURBS elements represent all rigid body motions and constant strain states exactly (see Hughes [14]). Consequently, structures assembled from compatible NURBS elements pass standard "patch tests" (see Hughes [14], chapters 3 and 4, for a description of patch tests).

3.3 Linear and nonlinear parameterizations

When dealing with NURBS, an important issue is the choice of the parameterization to be used. Take as an example a 1D domain: the simplest (and more natural) option is to employ a linear parameterization, but in some situations a nonlinear choice can be more suitable.

The isogeometric procedure originally proposed by Hughes *et al.* [15] is based on a distribution of control points which leads to a linear parameterization (i.e., constant Jacobian determinant), but in Cottrell *et al.* [7] it has been shown that when studying structural vibrations a nonlinear parameterization, such that the control points are uniformly spaced, gives better results. In Figure 4, we show the 1D distribution of 21 control points obtained for the two cases using cubic NURBS (top), along with plots of the corresponding parameterization $x = x(\xi)$ and Jacobian

$J(\xi) = \dfrac{\mathrm{d}\, x(\xi)}{\mathrm{d}\, \xi}$ (bottom). Subsequently, we will refer to this choice, in which control points are uniformly distributed, as "nonlinear parameterization", in contrast with the linear one.

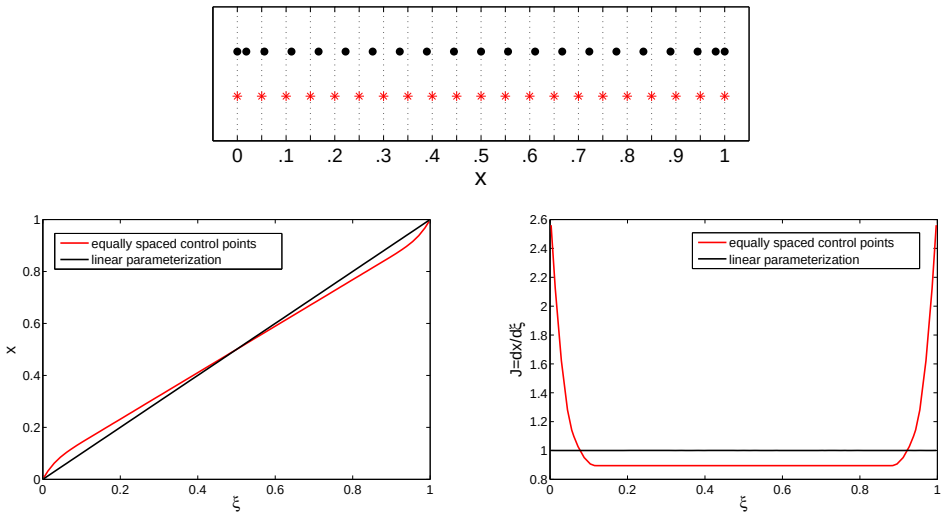

Fig. 4. 1D case: linear versus nonlinear parameterization determined by uniformly-spaced control points (cubic NURBS, 21 control points). Top: distribution of control points; dots correspond to linear parameterization control points and asterisks to uniformly-spaced control points. Bottom: plot of the parameterization (left) and of its Jacobian (right) for the two cases.

Finally, referring to the 2D case, we present in Figure 5 the example of a control net and mesh (i.e., the physical representation of the elements) of a square physical domain, obtained using $p = q = 4$ and 11×11 control points for both the linear and the nonlinear parameterizations.

3.4 k-method and p-method

We conclude this section on isogeometric analysis by briefly pointing out what we mean in this paper by the terms "*k*-method" and "*p*-method". Referring to the already cited *k*- and *p*-refinement strategies, we define the *k*-method as the analysis method exploiting the full continuity across the elements allowed by NURBS basis functions (i.e., C^{p-1} for a degree p NURBS). In the following we will simply label this method as "NURBS". Instead, we define the *p*-method as the analysis method where only C^0-continuity is enforced across elements (this can be obtained with isogeometric analysis by repeating the knots of a degree p NURBS $p-1$ times). This approach, used in combination with a linear parameterization, is equivalent to classical hp-finite element methods, and in the following we will simply label it as "FEM".

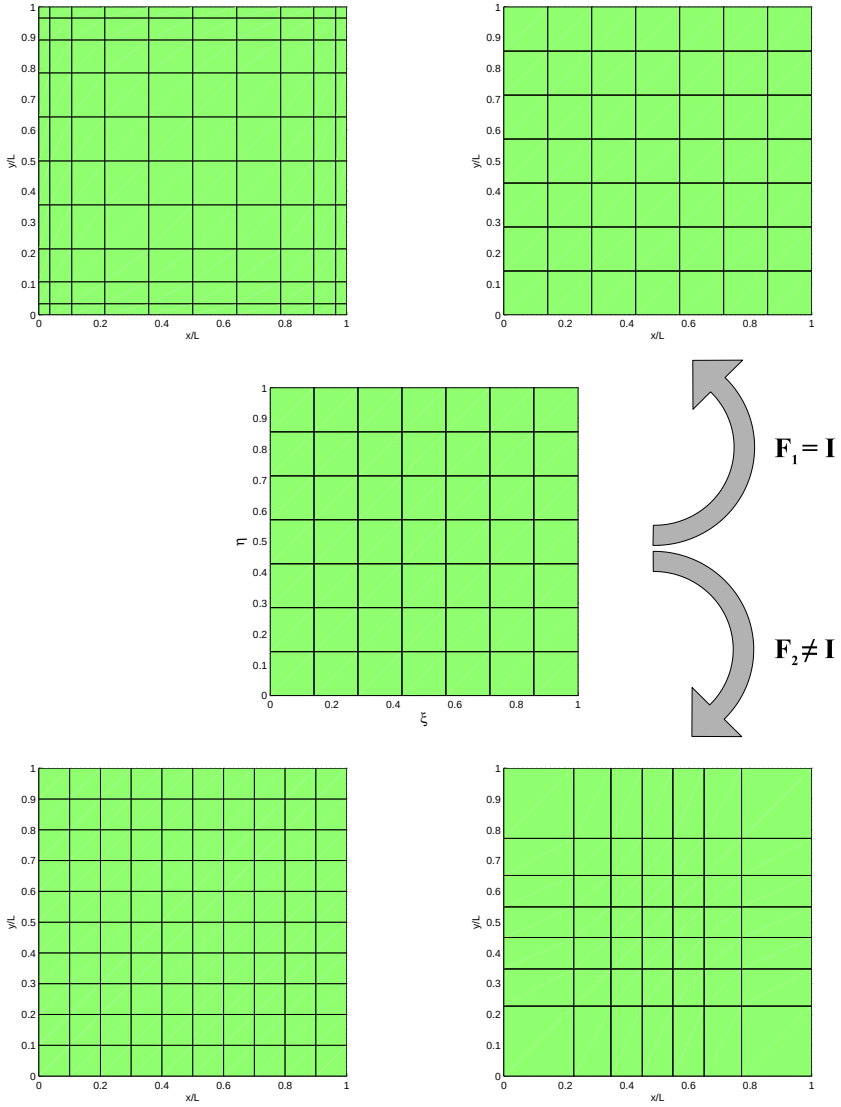

Fig. 5. 2D case: linear versus nonlinear parameterization determined by uniformly-spaced control points ($p = q = 4$, 11×11 control points). Top: control net (left) and mesh (right) obtained employing the linear parameterization, both plotted on the *physical domain*. Middle: mesh on the *parent domain*. Bottom: control net (left) and mesh (right) obtained employing the nonlinear parameterization, both plotted on the *physical domain*.

4 Analytical study in one dimension

In this section, we carry out some analytical computations for finding the discrete spectrum for structural vibrations (spectrum analysis) and the dispersion relation for wave propagation (dispersion analysis), and we discuss the similarity between the two frameworks. We first deal with the case of an approximation with linear elements, for which *k*- and *p*-methods coincide. Then, we discuss the extension of the results to higher order approximations, for both methods. This section is partly

based on [1, 12–14, 16, 22].

4.1 Linear approximation

4.1.1 Spectrum analysis

In this section, we solve the generalized discrete eigenproblem (3) associated to a linear approximation on the one-dimensional domain $(0, L)$, and study the error between discrete and exact solutions. We employ a uniform mesh $0 = x_0 < x_1 < \ldots < x_A < \ldots < x_{N+1} = L$, where the number of elements is $n_{el} = N + 1$ and the mesh-size is $h = L/n_{el}$.

Considering homogeneous Dirichlet (fixed-fixed) boundary conditions, the eigenproblem (3) can be written as

$$\frac{1}{h}(\phi_{A-1}-2\phi_A+\phi_{A+1})+\frac{h(\omega^h)^2}{6}(\phi_{A-1}+4\phi_A+\phi_{A+1}) = 0, \quad A = 1, \ldots, N, \tag{19}$$

$$\phi_0 = \phi_{N+1} = 0, \tag{20}$$

where N is the total number of degrees-of-freedom, and $\phi_A = \phi^h(x_A)$ is the nodal value of the discrete normal mode at node x_A. Equation (19) constitutes a linear homogeneous recurrence relation of order 2, whose solutions (ignoring, for now, the boundary conditions (20)) are linear combinations of exponential functions $\phi_A = (\rho_1)^A$ and $\phi_A = (\rho_2)^A$, where ρ_1 and ρ_2 are the distinct roots of the characteristic polynomial

$$(1 - 2\rho + \rho^2) + \frac{(\omega^h h)^2}{6}(1 + 4\rho + \rho^2) = 0. \tag{21}$$

Actually, (21) admits distinct roots when $\omega^h h \neq 0, \sqrt{12}$; for $\omega^h h = 0$, (21) admits the double root $\rho = 1$ (in this case, solutions of (19) are combinations of $\phi_A \equiv 1$ and $\phi_A = A$, that is, the affine functions), while for $\omega^h h = \sqrt{12}$ there is a double root $\rho = -1$ (and solutions of (19) are combinations of $\phi_A = (-1)^A$ and $\phi_A = A(-1)^A$). Observe that, in general, $\rho_2 = \rho_1^{-1}$.

For the purpose of spectrum analysis, we are interested in $0 < \omega^h h < \sqrt{12}$, which we assume for the remainder of this section. In this case, $\rho_{1,2}$ are complex conjugate (we assume $Im(\rho_1) \geq 0$) and of unit modulus. Moreover, in order to compare the discrete spectrum to the exact spectrum, it is useful to represent the solutions of (19) as linear combinations of $e^{\pm \mathrm{i} A\omega h}$ (that is, $\phi_A = C_- e^{-\mathrm{i}A\omega h} + C_+ e^{\mathrm{i}A\omega h}$), by introducing ω such that $e^{\mathrm{i}\omega h} = \rho_1$. With this hypothesis, ω is real and, because of periodicity, we restrict to $0 \leq \omega h \leq \pi$. Using this representation in (21) and using the identity $2\cos(\alpha) = e^{\mathrm{i}\alpha} + e^{-\mathrm{i}\alpha}$, after simple computations the relation between

ωh and $\omega^h h$ is obtained:

$$\frac{(\omega^h h)^2}{6}(2+\cos(\omega h)) - (1-\cos(\omega h)) = 0. \tag{22}$$

Solving for $\omega^h h \geq 0$, we get

$$\omega^h h = \sqrt{6\frac{1-\cos(\omega h)}{2+\cos(\omega h)}}. \tag{23}$$

Taking now into account the boundary conditions, non-null solutions ϕ_A of (19)–(20) exist when $\omega = \pi/L, 2\pi/L, \ldots, N\pi/L$. Indeed, for $\omega h = n\pi h/L \equiv n\pi/(N+1)$, and $C_- = -C_+$, the solution

$$\phi_A = C\frac{e^{+\mathrm{i}An\pi/(N+1)} - e^{-\mathrm{i}An\pi/(N+1)}}{2\mathrm{i}} \equiv C\sin\left(\frac{An\pi}{N+1}\right) \tag{24}$$

vanishes when $A = 0$ or $A = N+1$.

Precisely, (24) is the n^{th} discrete normal mode, associated to the corresponding n^{th} discrete natural frequency ω^h, given by (23):

$$\omega^h = \frac{N+1}{L}\sqrt{6\frac{1-\cos(n\pi/(N+1))}{2+\cos(n\pi/(N+1))}}. \tag{25}$$

Observe that (25) returns the frequencies ω^h in increasing order with respect to n. Figure 6 shows the dimensionless discrete natural frequencies $\omega^h h$, for $N = 9$ degrees-of-freedom. They are represented by points lying on the graph of $\omega^h h$ versus $\omega h/\pi$, given by (23). The abscissa $\omega h/\pi$ is equivalent to the scaled wave-number $n/(N+1)$.

As is known, the n^{th} discrete mode $\phi_A = C\sin(An\pi/(N+1))$ is the nodal interpolant of the n^{th} exact mode $\phi(x) = C\sin(n\pi x/L)$, whose natural frequency is $\omega = n\pi/L$. The quantity $\dfrac{\omega^h}{\omega} - 1 = \dfrac{\omega^h - \omega}{\omega}$ represents the relative error for the natural frequency. The plot of

$$\frac{\omega^h}{\omega} = \frac{1}{\omega h}\sqrt{6\frac{1-\cos(\omega h)}{2+\cos(\omega h)}}, \tag{26}$$

straightforwardly derived from (23), is shown in Figure 10.

4.1.2 Dispersion analysis

We obtain here the discrete dispersion relation for linear approximation. We consider the Helmholtz equation (6) on the infinite domain (line), and its discretization

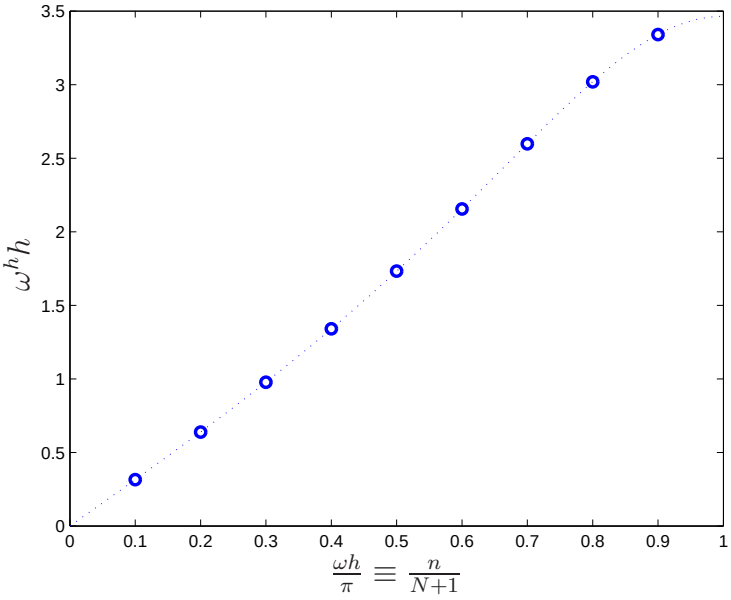

Fig. 6. Analytically-computed (discrete) natural frequencies for linear approximation, $N = 9$. The dimensionless frequencies lie on the graph (dotted line) of relation (23).

(7) on the numerical grid $x_A = hA$, $A \in \mathbb{Z}$. The resulting stencil equation is

$$\frac{1}{h}(u_{A-1} - 2u_A + u_{A+1}) + k^2\frac{h}{6}(u_{A-1} + 4u_A + u_{A+1}) = 0, \quad \forall A \in \mathbb{Z}. \tag{27}$$

As we described in Section 2.2, the standard dispersion analysis consists of comparing the wave-numbers of the exact and discrete solutions. We recall that the exact solutions of the Helmholtz equation are linear combinations of $u(x) = e^{\pm \mathrm{i}kx}$. Also, the discrete solutions, that is, solutions of the stencil equation (27), are combinations of exponentials (as we have seen in the previous section for (19), which is analogous to (27)): following the notation which is common in the context of dispersion analysis, the discrete solutions are written as

$$u_A \equiv u^h(x_A) = C_- e^{-\mathrm{i}k^h hA} + C_+ e^{\mathrm{i}k^h hA}, \tag{28}$$

denoting by k^h the discrete wave-number. In general, $k^h \in \mathbb{C}$, and is uniquely determined under the condition $0 \leq Re(k^h h) \leq \pi$. Inserting (28) into (27), the relation between k and k^h is obtained (analogously to (22)) as

$$\frac{(kh)^2}{6}(2 + \cos(k^h h)) - (1 - \cos(k^h h)) = 0. \tag{29}$$

In this context, one is usually interested in solving (29) with respect to $k^h h$. The first step is

$$\cos(k^h h) = \frac{6 - 2(kh)^2}{6 + (kh)^2}, \tag{30}$$

where it is easily seen that (since $kh \geq 0$)

$$\left|\frac{6-2(kh)^2}{6+(kh)^2}\right| \leq 1 \quad \Leftrightarrow \quad kh \leq \sqrt{12}.$$

Then, for $kh \leq \sqrt{12}$ the discrete wave-number is real and given by

$$k^h h = \arccos\left(\frac{6-2(kh)^2}{6+(kh)^2}\right); \tag{31}$$

when $kh > \sqrt{12}$, $k^h h$ can be obtained as in (31), but $\arccos(\cdot)$ has to be understood as the complex arc-cosine (see [22]). The non-zero imaginary part of $k^h h$ produces an amplitude modulation of the discrete solutions which is, clearly, an unphysical feature of the numerical solution. However, for linear elements, it happens when reaching the *resolution limit*, which corresponds to the largest wave-number that the numerical mesh can represent (before aliasing occurs). For linear elements, the resolution limit is $k^h h = \pi$.

The plots of $Re(k^h h)$ and $Im(k^h h)$ versus kh are shown in Figure 7 (observe that kh is represented on the ordinate). The amplitude spectrum, that is, $|u_A|/|u_{A+1}| \equiv e^{Im(k^h h)}$ versus kh (assuming $u_A = e^{\mathrm{i}k^h hA}$), is presented in Figure 8.

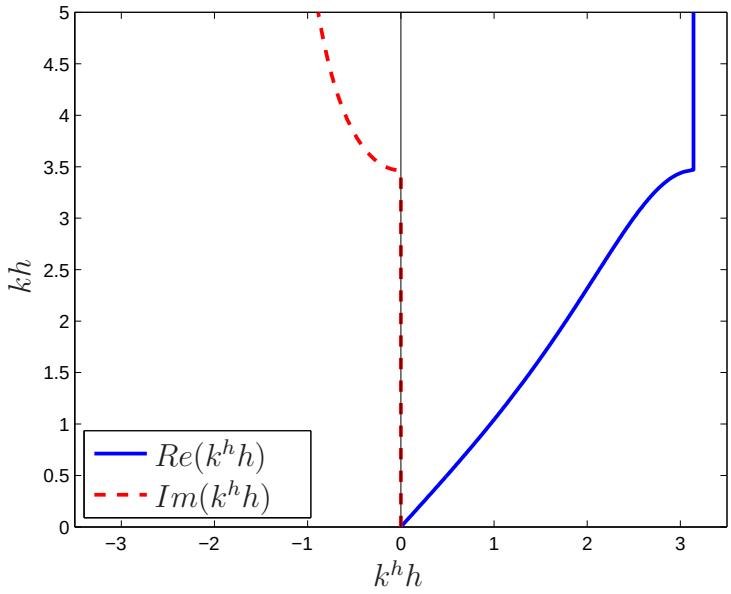

Fig. 7. Analytically-computed (discrete) wave-number for linear approximation.

The dispersion error $(k^h - k)/k = k^h/k - 1$ is typically displayed in the literature (e.g., see [12]) by plotting the quantity k^h/k versus $k^h h$, for $k^h h$ real. This is

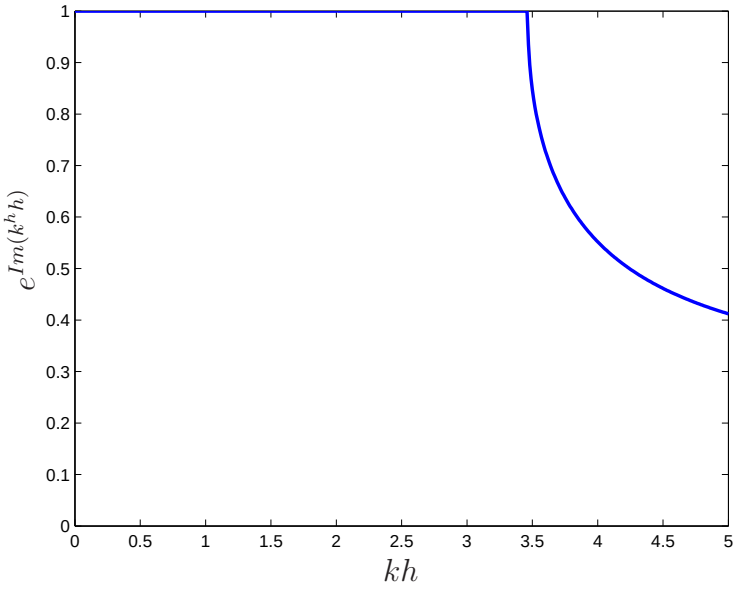

Fig. 8. Amplitude spectrum for linear approximation.

obtained from (29) as

$$\frac{k^h}{k} = \frac{k^h h}{\sqrt{6\dfrac{1-\cos(k^h h)}{2+\cos(k^h h)}}}, \tag{32}$$

and is shown in Figure 9.

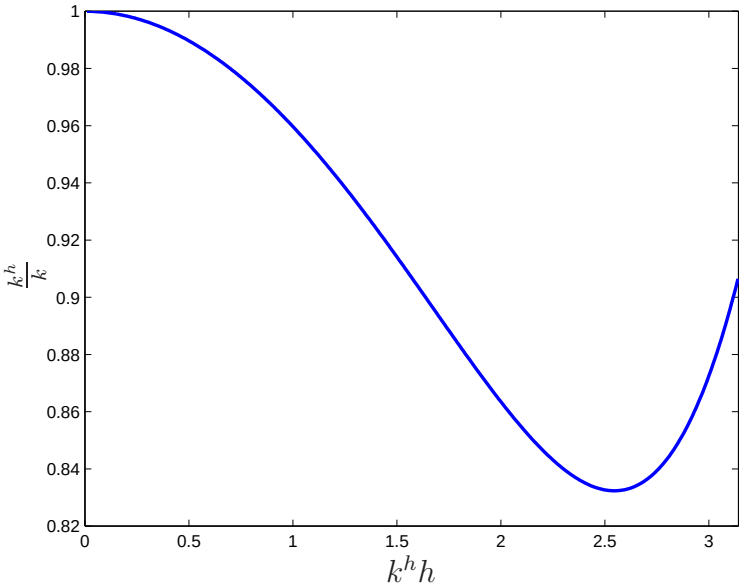

Fig. 9. Discrete-to-exact wave-number ratio for linear approximation.

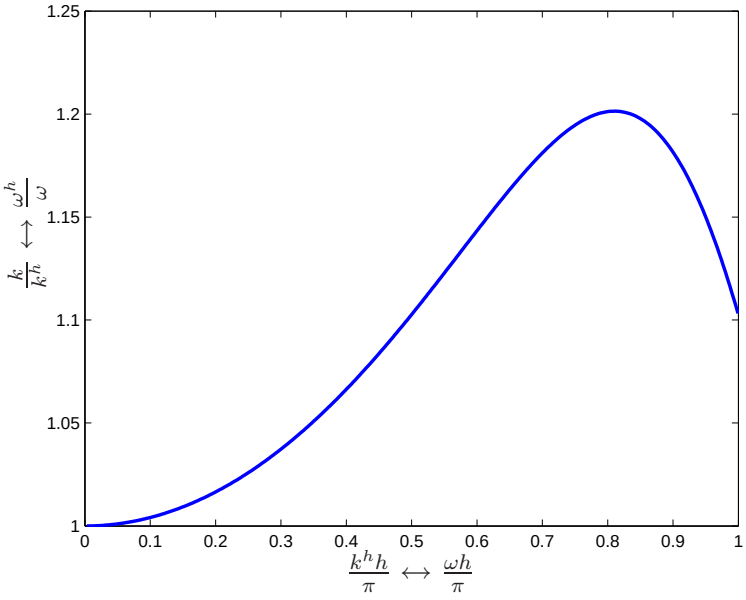

Fig. 10. Unified dispersion and spectrum analysis for linear approximation.

4.1.3 Duality Principle

Note that (32) is the reciprocal of expression (26), written in terms of different quantities: ω corresponds to k^h while ω^h corresponds to k.

Indeed, it is clear from Section 4.1.1–4.1.2 that spectrum analysis is equivalent to dispersion analysis in the regime where k^h is real: switching from one field to the other is just a matter of exchanging notation, from the mathematical viewpoint.

From now on, we will represent the dispersion error by plotting the ratio k/k^h versus $k^h h$. While this is not common in literature, it is suitable for unifying dispersion and spectrum analysis (see Figure 10).

Remark 1 *Figure 10 can be obtained numerically, instead of analytically. After numerically computing the spectrum, with eigenvalues sorted in increasing order, and then the frequencies of the discrete system, each discrete frequency is divided by the corresponding exact frequency $n\pi/L$. This gives ω^h/ω, with correct association of discrete to exact modes. In this case, the scaled mode number $n/(N+1)$ has to be represented as the abscissa.*

4.2 Higher order p-method

We have seen in the previous section that, for linear elements, spectrum and dispersion analysis are equivalent. This holds for the p-method with higher order elements as well, though the analysis becomes more technical. We discuss first, and in more

detail, the simpler case of quadratic elements.

We start by focusing on dispersion analysis. Therefore, we take into consideration the Helmholtz equation on the infinite line and its discretization by quadratic finite elements on the uniform grid $\ldots < x_A < x_{A+1/2} < x_{A+1} < \ldots$, where $x_A = hA$ (for $A \in \mathbb{Z}$) are the element-endpoint nodes and $x_{A+1/2} = h(A + 1/2)$ (for $A \in \mathbb{Z}$) are the mid-point nodes. On this mesh, we consider the usual nodal basis, depicted in Figure 11. The corresponding stencil equation is different for element-endpoint

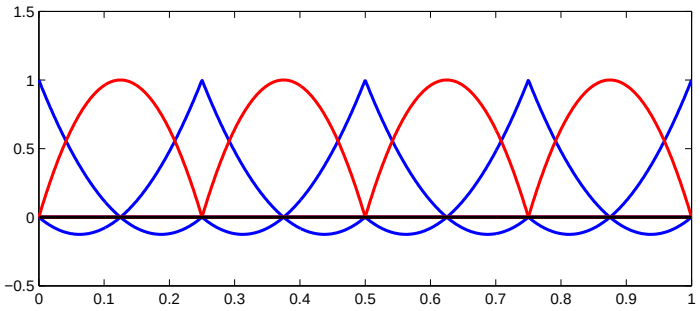

Fig. 11. Basis functions for the quadratic p-method.

degrees-of-freedom and bubble (internal to element) degrees-of-freedom: one has

$$\begin{aligned}&\frac{1}{3h}(-u_{A-1} + 8u_{A-1/2} - 14u_A + 8u_{A+1/2} - u_{A+1})\\&+ k^2\frac{h}{30}(-u_{A-1} + 2u_{A-1/2} + 8u_A + 2u_{A+1/2} - u_{A+1}) = 0, \quad \forall A \in \mathbb{Z}.\end{aligned} \tag{33}$$

and

$$\frac{1}{3h}(8u_A - 16u_{A+1/2} + 8u_{A+1}) + k^2\frac{h}{30}(2u_A + 16u_{A+1/2} + 2u_{A+1}) = 0, \quad \forall A \in \mathbb{Z}, \tag{34}$$

respectively. One could look for a solution of (33)–(34) at the element-endpoint and bubble nodes (see, for example, [22, §3.2.4]). However, a simpler and more common way to proceed consists of calculating the bubble degrees-of-freedom as

$$u_{A+1/2} = \frac{40 + (kh)^2}{8(10 - (kh)^2)}(u_A + u_{A+1}), \tag{35}$$

and eliminating them, obtaining a system of equations for u_A, $A \in \mathbb{Z}$, which is

$$\begin{aligned}&\frac{1}{3h}\left[\left(\frac{30 + 2(kh)^2}{10 - (kh)^2}\right)u_{A-1} + \left(\frac{-60 + 16(kh)^2}{10 - (kh)^2}\right)u_A + \left(\frac{30 + 2(kh)^2}{10 - (kh)^2}\right)u_{A+1}\right]\\&+ k^2\frac{h}{30}\left[\left(\frac{5(kh)^2}{40 - 4(kh)^2}\right)u_{A-1} + \left(\frac{200 - 15(kh)^2}{20 - 2(kh)^2}\right)u_A + \left(\frac{5(kh)^2}{40 - 4(kh)^2}\right)u_{A+1}\right] = 0,\end{aligned} \tag{36}$$

Remark 2 *The bubble elimination is not possible when the bubble equation (34) is singular for* $u_{A+1/2}$*. We refer to this situation as* bubble resonance*. It occurs for*

$$kh = \sqrt{10}. \tag{37}$$

Observe that (36) is a homogeneous linear recurrence equation of order 2, as for the linear case (27). Then, its solutions can be written as

$$u_A = C_- e^{-\mathrm{i}k^h hA} + C_+ e^{\mathrm{i}k^h hA}, \qquad \forall A \in Z. \tag{38}$$

Substituting (38) into (36), one obtains

$$\cos(k^h h) = \frac{3\,kh^4 - 104\,kh^2 + 240}{kh^4 + 16\,kh^2 + 240}. \tag{39}$$

Given kh, there is only one solution $k^h h$ to (39) if we restrict to $0 \leq Re(k^h h) \leq \pi$; this is

$$k^h h = \arccos\left(\frac{3\,kh^4 - 104\,kh^2 + 240}{kh^4 + 16\,kh^2 + 240}\right). \tag{40}$$

As for the linear case, if the right hand side of (39) is, in modulus, smaller than or equal to 1, then $k^h h$ is real (see the left plot of Figure 12). From (40) and Figure

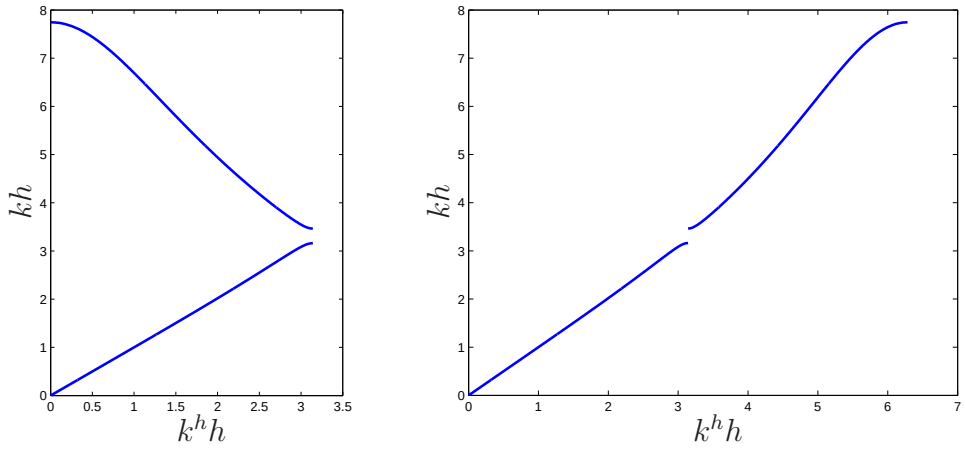

Fig. 12. Analytically-computed (discrete) wave-number for quadratic p-method, and $k^h h$ real. Relation (40) is plotted on the left, and relation (41) on the right.

12 (left), it is seen that each real value of $k^h h$ is associated with two values of kh, on two different branches, termed *acoustical* and *optical* (cf. [3]). This means that the solution at the endpoint-element nodes of the grid is the same for the two corresponding kh's; however, the bubble degrees-of-freedom (given by (35)) are different for the two cases, which means that the two discrete solutions (at element-endpoint and bubble nodes) are different. From (40), it is found that $kh \in [0, \sqrt{10}]$ for the acoustical branch and $kh \in [\sqrt{12}, \sqrt{60}]$ for the optical branch.

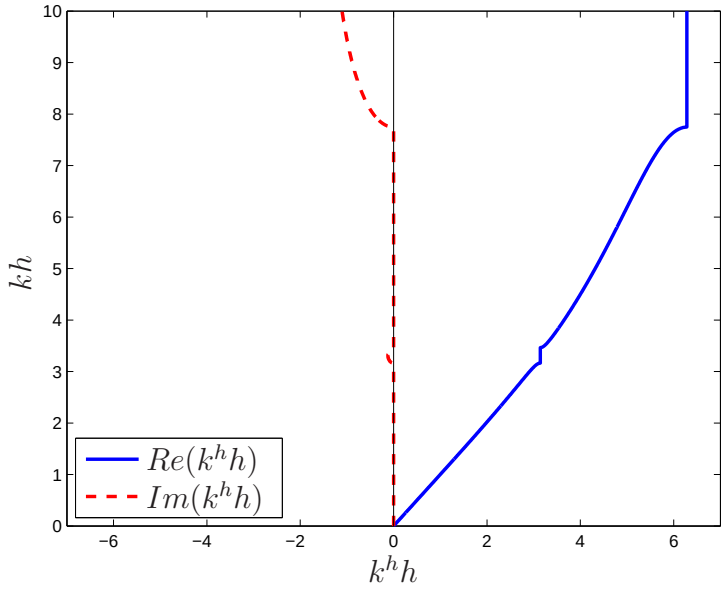

Fig. 13. Analytically-computed (discrete) wave-number for quadratic p-method.

A better representation of the relation $k^h h$ versus kh is derived from (39) as follows. For the optical branch, that is, for $kh \geq \sqrt{12}$, thanks to the even parity and periodicity of the cosine function, we represent the discrete wave-number in the range $\pi \leq Re(k^h h) \leq 2\pi$. Then, we set

$$k^h h = \begin{cases} \arccos\left(\dfrac{3\,kh^4 - 104\,kh^2 + 240}{kh^4 + 16\,kh^2 + 240}\right) & \text{for } kh < \sqrt{12}, \\ 2\pi - \arccos\left(\dfrac{3\,kh^4 - 104\,kh^2 + 240}{kh^4 + 16\,kh^2 + 240}\right) & \text{for } kh \geq \sqrt{12}. \end{cases} \tag{41}$$

This results in a one-to-one monotone relation between kh and the real values of $k^h h$, plotted in Figure 12 (right), which is consistent with the physical expectation and is useful in view of spectrum analysis. Moreover, $k^h h = 2\pi$ plays the role of resolution limit of the complete numerical grid (considering both bubble and element-endpoint nodes).

Allowing complex wave-numbers in (41), Figure 13 is obtained. Notice that $Im(k^h h)$ is not only zero for $kh > \sqrt{60}$ but also in between the two branches, for $\sqrt{10} < kh < \sqrt{12}$. This interval is called a *stopping band* and its effect on the numerical solution will be discussed in Section 6.2.1. The amplitude spectrum is shown in Figure 14.

We now turn to spectrum analysis, and consider the eigenproblem (3) on the domain $(0, L)$. The mesh restricts to $0 = x_0 < \ldots < x_{A-1/2} < x_A < x_{A+1/2} < \ldots < x_{n_{el}} = L$. The mesh-size is $h = L/n_{el}$. We have therefore $n_{el} + 1$ element-endpoint nodes, including x_0 and $x_{n_{el}}$, and n_{el} bubble nodes. Taking into account

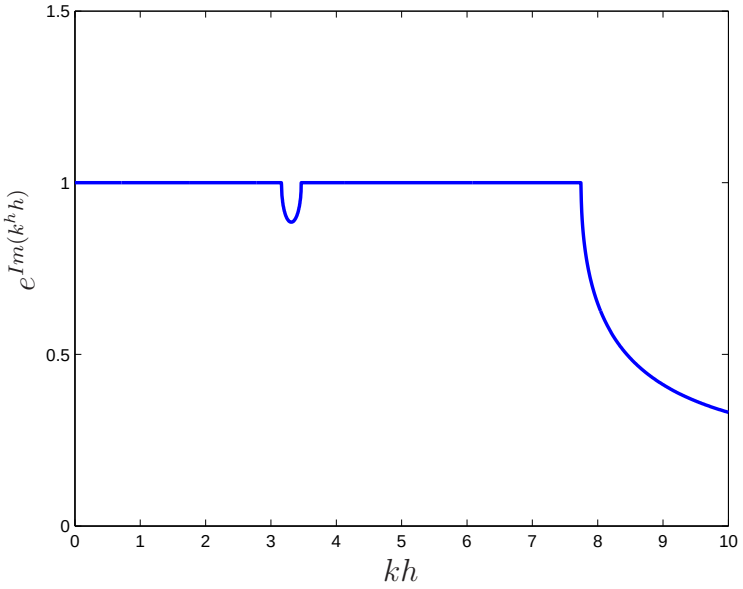

Fig. 14. Amplitude spectrum for quadratic p-method.

the homogeneous Dirichlet boundary conditions, there are $N = 2n_{el} - 1$ degrees-of-freedom. Based on the previous study of the Helmholtz equation (33)–(34), we assume $\omega^h h \neq \sqrt{10}$ and perform the bubble elimination, leading to the following equation for the element-endpoint degrees-of-freedom: for $A = 1, \ldots, n_{el} - 1$

$$\begin{aligned}
&\frac{1}{3h}\left[\left(\frac{30+2(\omega^h h)^2}{10-(\omega^h h)^2}\right)\phi_{A-1} + \left(\frac{-60+16(\omega^h h)^2}{10-(\omega^h h)^2}\right)\phi_A \right.\\
&\qquad \left. + \left(\frac{30+2(\omega^h h)^2}{10-(\omega^h h)^2}\right)\phi_{A+1}\right]\\
&+ k^2\frac{h}{30}\left[\left(\frac{5(\omega^h h)^2}{40-4(\omega^h h)^2}\right)\phi_{A-1} + \left(\frac{200-15(\omega^h h)^2}{20-2(\omega^h h)^2}\right)\phi_A \right.\\
&\qquad \left. + \left(\frac{5(\omega^h h)^2}{40-4(\omega^h h)^2}\right)\phi_{A+1}\right] = 0.
\end{aligned} \tag{42}$$

We also have the boundary conditions $\phi_0 = \phi_{n_{el}} = 0$. Clearly, (42) is the counterpart of (36). We proceed now using the dispersion analysis results of the present section, invoking the duality principle, that is, the correspondence $\omega^h \leftrightarrow k$ and $\omega \leftrightarrow k^h$, and reasoning as for spectrum analysis in the linear case (see Section 4.1.1).

Normal modes at element-endpoint nodes can be written as $\phi_A = C_- e^{-i\omega h A} + C_+ e^{\mathrm{i}\omega h A}$; the boundary condition $\phi_0 = 0$ determines $C_- = -C_+$, while $\phi_{n_{el}} = 0$ if $\frac{\omega L}{\pi} \in \mathbb{Z}$. Observe that the complex values of ωh are not of interest in this case. The

relation between $\omega^h h$ and ωh is (analogous to (39))

$$\cos(\omega h) = \frac{3\,(\omega^h h)^4 - 104\,(\omega^h h)^2 + 240}{(\omega^h h)^4 + 16\,(\omega^h h)^2 + 240}. \tag{43}$$

The natural frequencies are obtained solving (43) with respect to $\omega^h h$. Unlike the linear case, this is a two-branch relation: there are two roots $\omega^h h \geq 0$ for any $\omega h \in \mathbb{R}$. As we have seen, a monotone $\omega^h h$ versus ωh relation is obtained representing the two branches in the range $\omega h \in [0, \pi]$ and $\omega h \in [\pi, 2\pi]$, respectively. Therefore, we associate to

$$\omega h = \frac{n\pi}{n_{el}}, \quad n = 1, \ldots n_{el} - 1, \tag{44}$$

the smallest positive root of (43), obtaining the acoustical branch, and we associate to

$$\omega h = \frac{n\pi}{n_{el}}, \quad n = n_{el} + 1, \ldots 2n_{el} - 1 \equiv N; \tag{45}$$

the highest root of (43), obtaining the optical branch. These roots are the natural frequencies that can be obtained by bubble elimination.

The frequency $\omega^h h = \sqrt{10}$, which gives bubble resonance (see Remark 2) has to be taken into consideration as well. Indeed, it is associated with the normal mode

$$\begin{aligned} \phi_A &= 0, & \forall A &= 0, \ldots, n_{el}, \\ \phi_{A+1/2} &= C(-1)^A & \forall A &= 0, \ldots, n_{el} - 1. \end{aligned} \tag{46}$$

Since $\omega^h h = \sqrt{10}$ is located between the two branches, this frequency is associated with mode number $n = n_{el}$. Notice that with this choice, all the normal modes at element endpoints are given by

$$\phi_A = C \sin\left(\frac{An\pi}{N+1}\right), \qquad A = 0, 1, \ldots n_{el}, \tag{47}$$

n being the mode number. Therefore, (47) interpolate of the exact modes (at element endpoint nodes).

Eventually, this results in a monotone ordering of all the natural frequencies of the discretized system, as shown in Figure 15 (for $N = 9$). The abscissa in Figure 15 is $\omega h/2\pi$, which corresponds to the scaled wave-number $n/(N+1)$.

The numerical error in the calculation of natural frequencies is visualized by the graph of ω^h/ω versus ωh. As for the linear case, it is the same graph of k/k^h versus $k^h h$, which reveals the dispersion error. The unified plot is shown in Figure 16.

What we have described for the case $p = 2$ can be easily generalized to higher order cases $p > 2$, in one space dimension. In general we have $p - 1$ bubbles per element, and then p branches and $p - 1$ stopping bands. See, for example, Figures 17 and 18 which refer to the case $p = 3$. In particular, assuming the resolution limit

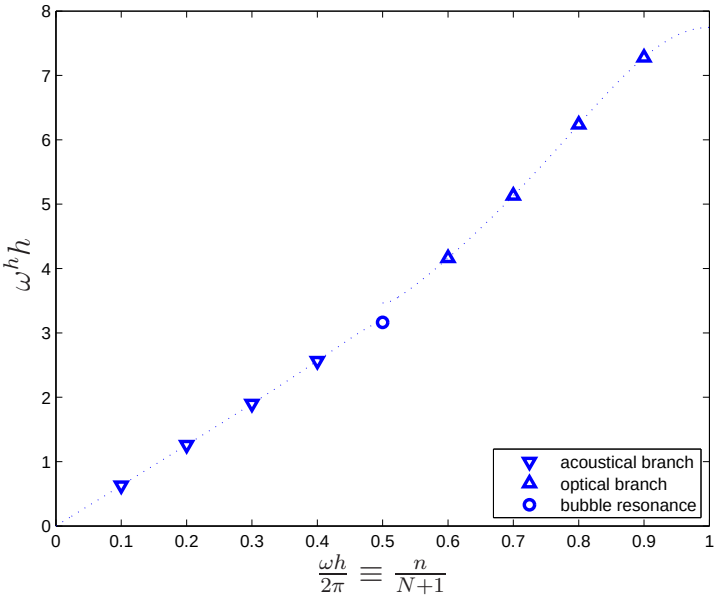

Fig. 15. Analytically-computed (discrete) natural frequencies for quadratic p-method ($N = 9$).

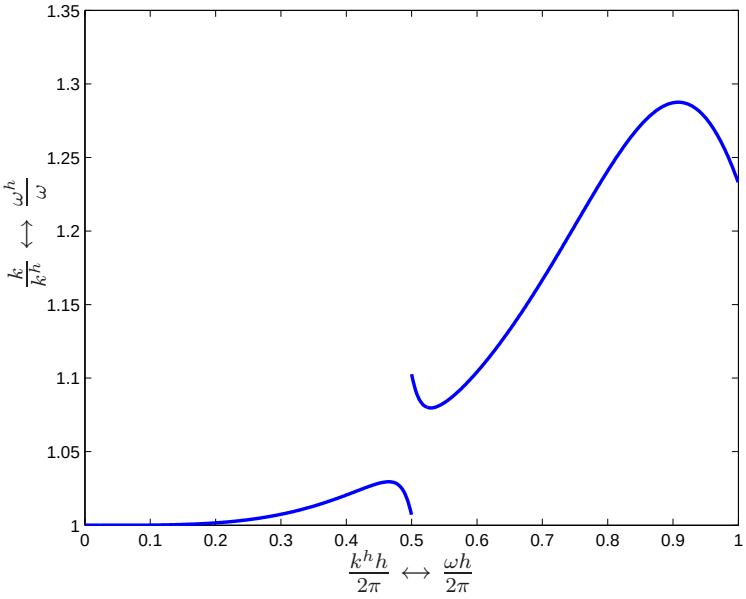

Fig. 16. Unified dispersion and spectrum analysis for quadratic p-method.

to be $k^h h \equiv \omega h = p\pi$, one can derive the monotone $\omega^h h$ versus ωh relation which is useful for the spectrum representation. There are also $p - 1$ natural frequencies associated to bubble resonance.

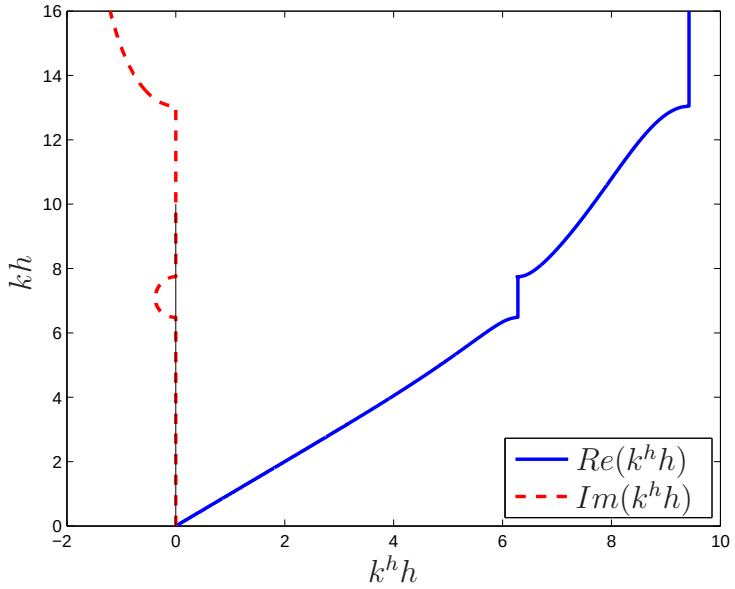

Fig. 17. Analytically-computed (discrete) wave-number for cubic p-method.

4.3 Higher order k-method

There is also a strict relation between spectrum and dispersion analysis for the k-method with higher-order elements. Again, for the sake of simplicity, we only discuss in detail the quadratic approximation, and briefly mention the extensions to $p > 2$ at the end of this section.

Considering the Helmholtz equation (7) on the infinite line, we denote now by $x_A = hA$, for $A \in \mathbb{Z}$, the sequence of h-spaced control points (giving a linear parameterization of the infinite line); the stencil equation is then

$$\begin{aligned} &\frac{1}{6h}(u_{A-2} + 2u_{A-1} - 6u_A + 2u_{A+1} + u_{A+2}) \\ &\quad + k^2 \frac{h}{120}(u_{A-2} + 26u_{A-1} + 66u_A + 26u_{A+1} + u_{A+2}) = 0, \quad \forall A \in \mathbb{Z}. \end{aligned} \tag{48}$$

Remember that, for the k-method, u_A denotes the coefficient in the basis expansion, which is no longer interpolatory. Another major difference from the cases considered in the previous sections is that (48) is a homogeneous recurrence relation of order 4. Because of its structure, its solutions can be written as linear combinations of the four solutions $e^{\pm \mathrm{i} k^h h A}$ and $e^{\pm \mathrm{i} \tilde{k}^h h A}$, where $k^h \neq \tilde{k}^h$ are uniquely determined under the assumption $0 \leq Re(k^h h) \leq \pi$, $0 \leq Re(\tilde{k}^h h) \leq \pi$ and $Im(\tilde{k}^h) < Im(k^h) \leq 0$. Notice that the space of discrete solutions has dimension 4, unlike the space of exact solutions ($e^{\pm \mathrm{i} k x}$) which has dimension 2. The values of $k^h h$ and $\tilde{k}^h h$ can be obtained from kh using (48). These are plotted in Figure

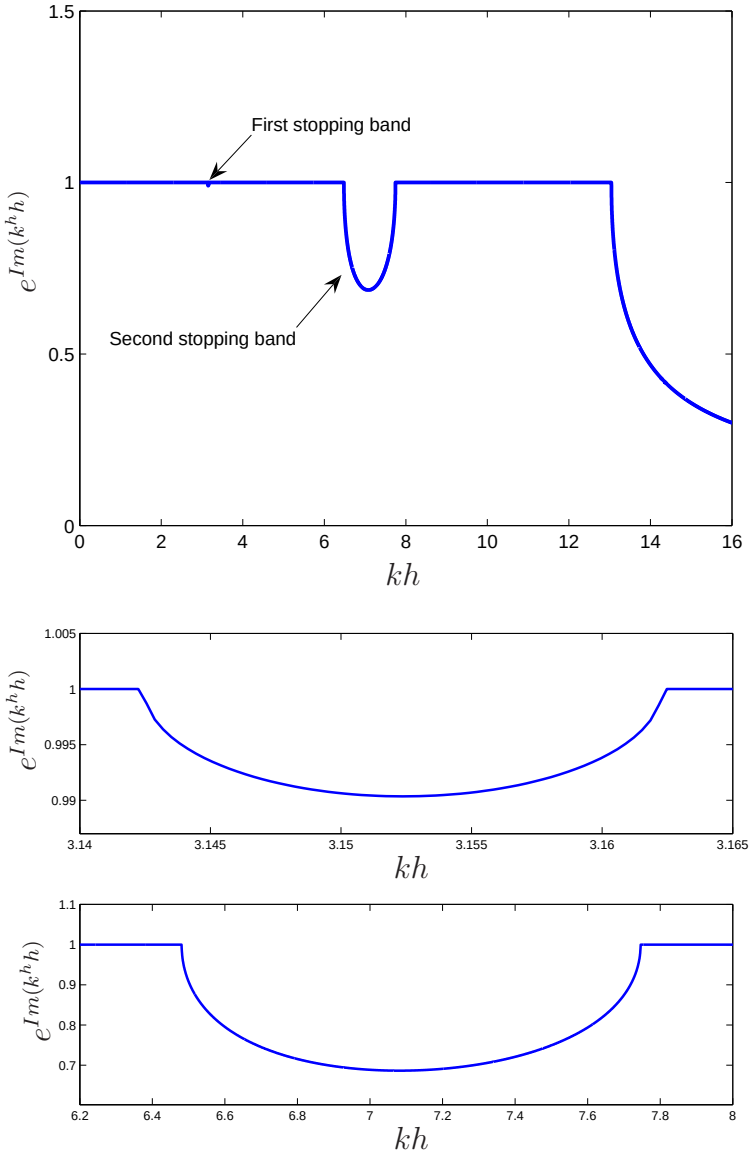

Fig. 18. Amplitude spectrum for cubic p-method (top) and detail of the two stopping bands.

19. It is seen that k^h is an approximation of the exact wave-number k ($k^h h \approx kh$ within the resolution range $k^h h \in [0, \pi]$), while $\tilde{k}^h$ is a numerical wave-number, associated with spurious evanescent waves of the form $u_A = C(-1)^A e^{\mp Im(\tilde{k}^h h)A}$.

The role of the spurious solutions of (48) is not fully clear. These solutions are irrelevant at low kh (in this case, the *a priori* error analysis guarantees the accuracy of the numerical solution) while they could affect the numerical solution at high kh. Nevertheless, in all the numerical tests we have performed (see Section 6.2), they did not appear, perhaps because they are so strongly attenuated. See Figure 20.

Therefore, for the purpose of the dispersion analysis, we only consider the relation

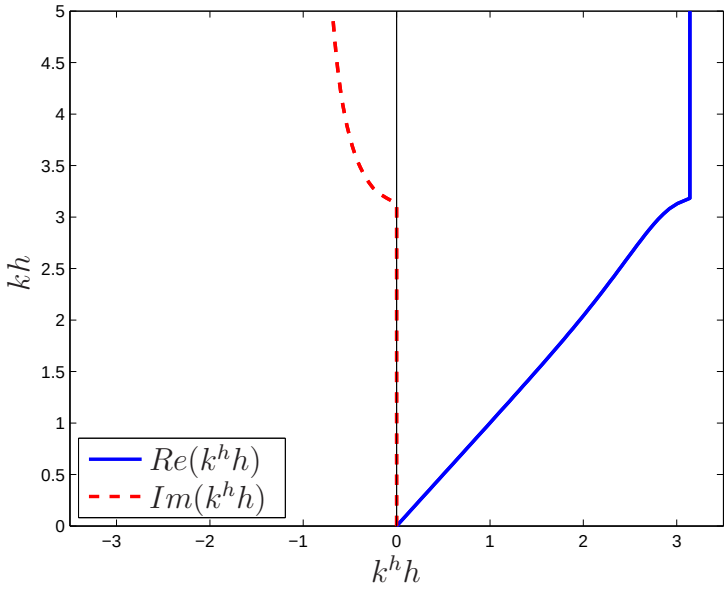

Fig. 19. Analytically-computed (discrete) wave-number for quadratic k-method.

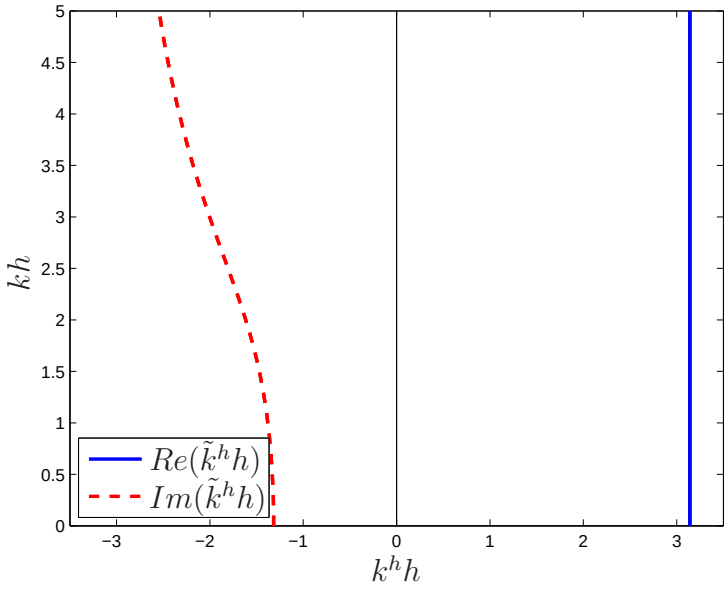

Fig. 20. Analytically-computed spurious wave-number for quadratic k-method.

k/k^h versus $k^h h$. After simple computations this is obtained from (48) as

$$\frac{k}{k^h} = \frac{1}{k^h h}\sqrt{\frac{20(2-\cos(k^h h)-\cos(k^h h)^2)}{16+13\cos(k^h h)+\cos(k^h h)^2}}, \tag{49}$$

and plotted in Figure 21.

Let us discuss now how the results above are related to spectrum analysis. Consider

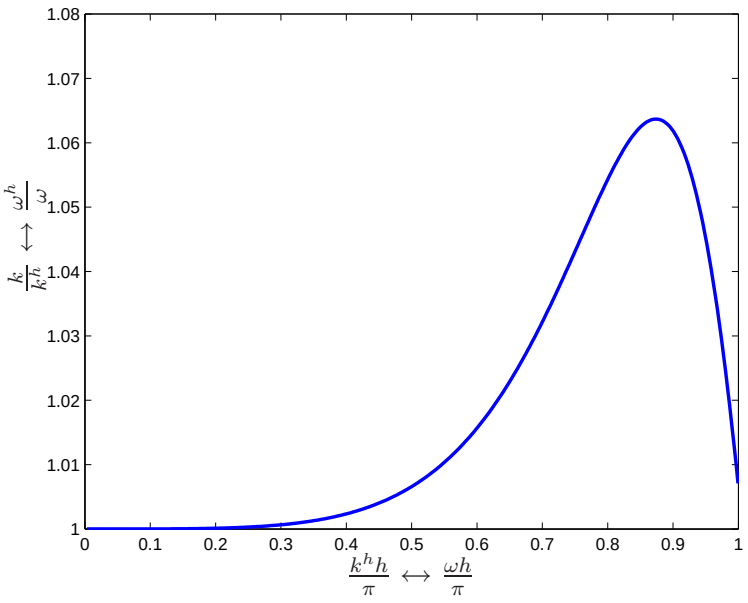

Fig. 21. Unified dispersion and spectrum analysis, for quadratic k-method.

the eigenvalue problem (3) on the interval $(0, L)$, on which we introduce $N+2$ control points associated to a linear parameterization. The control points are uniformly spaced, at distance h, only in the interior portion of the domain, while they get closer to each other at the endpoints of the domain $(0, L)$, as shown in Figure 4. On the other hand, the space of discrete functions is made of piecewise quadratic polynomials on a uniform mesh with knot spacing h [1], with global C^1 regularity (see Figure 22). In this cases, the discrete problem (3) reads

$$\begin{cases} \dfrac{1}{6h}(6\phi_0 - 8\phi_1 + \phi_2 + \phi_3) + \dfrac{h(\omega^h)^2}{120}(14\phi_0 + 40\phi_1 + 25\phi_2 + \phi_3) = 0, \\ \dfrac{1}{6h}(2\phi_0 + \phi_1 - 6\phi_2 + 2\phi_3 + \phi_4) + \dfrac{h(\omega^h)^2}{120}(2\phi_0 + 25\phi_1 + 66\phi_2 + 26\phi_3 + \phi_4) = 0, \end{cases} \tag{50}$$

$$\begin{cases} \forall A = 3, \dots, N-2, \\ \dfrac{1}{6h}(\phi_{A-2} + 2\phi_{A-1} - 6\phi_A + 2\phi_{A+1} + \phi_{A+2}) \\ \quad + \dfrac{h(\omega^h)^2}{120}(\phi_{A-2} + 26\phi_{A-1} + 66\phi_A + 26\phi_{A+1} + \phi_{A+2}) = 0, \end{cases} \tag{51}$$

[1] Note, h here corresponds to the knot spacing in physical space. Previously, when analyzing quadratic finite elements, we adopted the usual convention that h represents the element length. Consequently, the h's in these two cases differ by a factor of 2.

$$\begin{cases} \dfrac{1}{6h}(\phi_{N-3} + 2\phi_{N-2} - 6\phi_{N-1} + \phi_N + 2\phi_{N+1}) \\ \quad + \dfrac{h(\omega^h)^2}{120}(\phi_{N-3} + 26\phi_{N-2} + 66\phi_{N-1} + 25\phi_N + 2\phi_{N+1}) = 0, \\ \dfrac{1}{6h}(\phi_{N-2} + \phi_{N-1} - 8\phi_N + 6\phi_{N+1}) \\ + \dfrac{h(\omega^h)^2}{120}(\phi_{N-2} + 25\phi_{N-1} + 40\phi_N + 14\phi_{N+1}) = 0 \end{cases} \tag{52}$$

along with the Dirichlet boundary conditions

$$\phi_0 = \phi_{N+1} = 0. \tag{53}$$

Substituting (53) into (50)–(52), this is an N-dimensional generalized eigenvalue problem.

The equations (51) for the interior degrees-of-freedom correspond to the stencil (48) we previously considered in the dispersion analysis. However, the boundary equations (50) and (52) are different, due to the different shape of the boundary basis functions (see Figure 22). The relation between the solutions of (48) and the

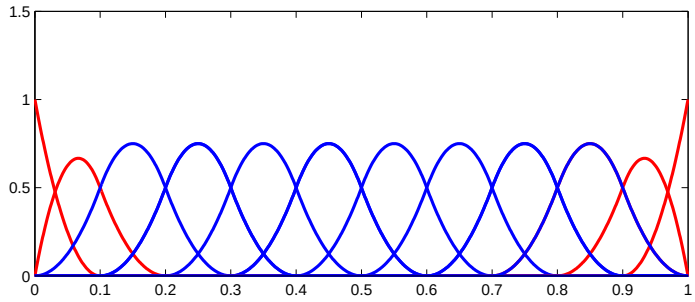

Fig. 22. Basis functions for the quadratic k-method

ones of (50)–(53), which is not trivial, is addressed in the following discussion. First, we deal with (51) and use the previous study of the Helmholtz equation (invoking the duality principle and change of notation $\omega^h \leftrightarrow k$, $\omega \leftrightarrow k^h$ and $\tilde{\omega} \leftrightarrow \tilde{k}^h$), to infer that the solutions of (51) are

$$\phi_A = C_+ e^{\mathrm{i}\omega h A} + C_- e^{-\mathrm{i}\omega h A} + \tilde{C}_+ e^{\mathrm{i}\tilde{\omega} h A} + \tilde{C}_- e^{-\mathrm{i}\tilde{\omega} h A}, \quad \forall A = 1, \ldots, N. \tag{54}$$

Inserting this expression into the boundary equations (50) and (52), and imposing the boundary conditions (53), one determines the four coefficients C_-, C_+, $\tilde{C}_-$, and $\tilde{C}_+$ in order that (54) is the solution of the entire system (50)–(53). The trivial solution corresponds to $C_- = C_+ = \tilde{C}_- = \tilde{C}_+ = 0$. The normal modes are instead the non-zero solutions, which exist for suitable $\omega^h h$ (giving the discrete natural frequencies) and corresponding ωh and $\tilde{\omega} h$. Precisely, the n^{th} normal mode turns

out to be [2]

$$\begin{cases} \phi_A = C \sin\left(n\pi \dfrac{A-1/2}{N}\right), \quad \forall A = 1, \ldots, N, \\ \phi_0 = \phi_{N+1} = 0, \end{cases} \tag{55}$$

that is, $\omega h = n\pi/N$, $C_- = C_+$ and $\tilde{C}_- = \tilde{C}_+ = 0$; the corresponding frequency is given by

$$\omega^h h = \sqrt{\frac{20(2 - \cos(\omega h) - \cos(\omega h)^2)}{16 + 13\cos(\omega h) + \cos(\omega h)^2}}. \tag{56}$$

Figure 23 shows the discrete frequencies for $N = 9$ degrees-of-freedom, together with the graph of (56). The abscissa is the scaled mode number $\omega h/\pi = n/N$. Notice that the present scaling of the mode number is different from the one adopted for linear and higher order p-methods in Sections 4.1.1 and 4.2.

Remark 3 *The spurious wave components $e^{\pm \mathrm{i}\tilde{\omega} h A}$ do not contribute to the normal modes (55).*

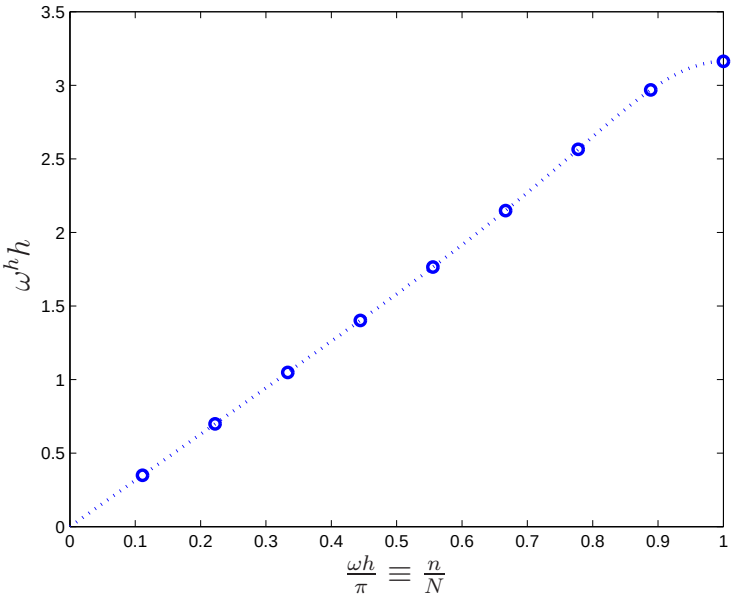

Fig. 23. Analytically-computed (discrete) natural frequencies for quadratic k-method ($N = 9$).

The case of higher order elements $p > 2$ is conceptually similar, though the higher is p, the more technical the analysis becomes. For dispersion analysis, the space of discrete solutions (of the Helmholtz equation) has dimension $2p$, with $2p - 2$ spurious (linearly independent) solutions. For the purpose of the spectrum analysis, one has to split the eigenvalue/eigenvector problem into boundary and interior (stencil)

[2] We emphasize that the ϕ_A's are the control variables and are not interpolated by the solution.

equations: the former are used to determine which solutions of the interior equations are compatible with the boundary conditions, thus giving admissible normal modes. They have a structure that is similar to (55) but the last $p-1$, for p odd, or $p-2$, for p even, correspond to evanescent waves, and are associated to "outlier frequencies" (see [7]).

The outlier frequencies disappear, for any p, when a nonlinear parameterization of the domain is adopted, through the uniform distribution of control points shown in Figure 4. This is observed numerically but a sound mathematical explanation is still missing. Indeed, in spectrum analysis the k-method with nonlinear parameterization exhibits a more complicated behavior than the k-method with linear parameterization. In Figure 24 the numerically computed ω^h/ω (see Remark 1) are plotted for $N = 3,\ 10,\ 30$ degrees-of-freedom: it is possible to notice that the points do not lie on an underlying curve independent of N. However, they converge towards the graph of the analytical relation (56), when $N \to \infty$. The same behavior is observed for $p > 2$ as well; the computed ω^h/ω versus the scaled mode number converges, for $N \to \infty$, towards the analytical relation obtained considering only the non-spurious solutions of the internal stencil equation.

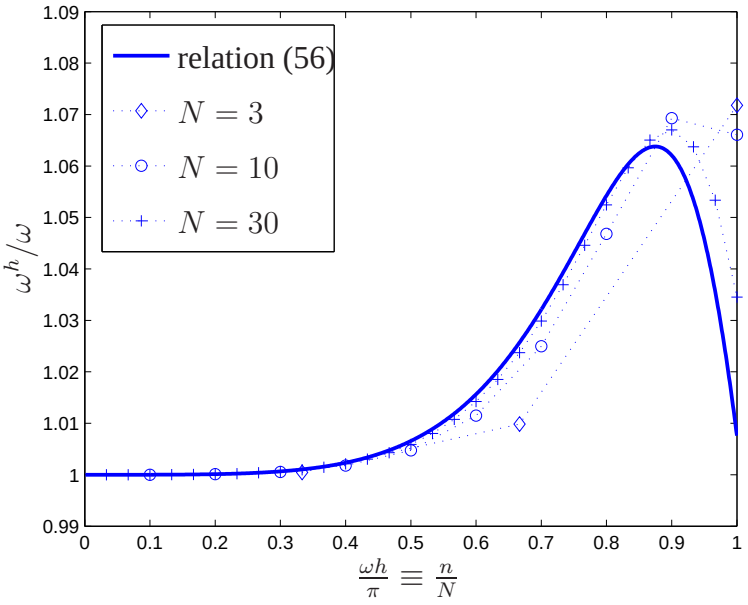

Fig. 24. Numerical spectrum analysis compared to the analytically-computed relation (56) for the quadratic k-method with nonlinear parameterization.

5 Analytical study in two dimensions

Spectrum and dispersion analysis can be put in relation in two, and more, dimensions as well. We discuss here the equivalence between the study of propagation of

numerical waves on the infinite grid and the study of discrete natural frequencies on a rectangular domain. At the discrete level, we only discuss the case of bilinear approximation, but the same concepts extend to the higher order p-method (using the techniques of, e.g., [9]), and k-method (dealing with the boundary equations as in the one-dimensional setting).

Discretizing the Helmholtz equation by bilinear approximation on the infinite uniform mesh of square elements of side length h, the discrete equations are

$$\begin{aligned}
&\frac{1}{3h}(-8u_{(A_1,A_2)} + u_{(A_1-1,A_2-1)} + u_{(A_1-1,A_2)} + u_{(A_1-1,A_2+1)} \\
&+ u_{(A_1,A_2-1)} + u_{(A_1,A_2+1)} + u_{(A_1+1,A_2-1)} + u_{(A_1+1,A_2)} + u_{(A_1+1,A_2+1)}) \\
&+ \frac{kh}{9}(4u_{(A_1,A_2)} + \frac{1}{4}u_{(A_1-1,A_2-1)} + u_{(A_1-1,A_2)} + \frac{1}{4}u_{(A_1-1,A_2+1)} + u_{(A_1,A_2-1)} \\
&+ u_{(A_1,A_2+1)} + \frac{1}{4}u_{(A_1+1,A_2-1)} + u_{(A_1+1,A_2)} + \frac{1}{4}u_{(A_1+1,A_2+1)}), \qquad \forall \mathbf{A} \in \mathbb{Z}^2,
\end{aligned} \tag{57}$$

where $u_{\mathbf{A}} \equiv u_{(A_1,A_2)}$ are the degrees-of-freedom with respect to the standard nodal basis.

The solutions of (57) are linear combinations of discrete plane waves $u_{\mathbf{A}} = e^{\mathrm{i}h\mathbf{k}^h\cdot\mathbf{A}}$, where (see, e.g., [9]) the discrete wave-number $\mathbf{k}^h = (k_1^h, k_2^h)$ satisfies

$$\begin{aligned}
&\left(\frac{8}{3} - \frac{4}{9}(kh)^2\right) - \left(\frac{2}{3} + \frac{2}{9}(kh)^2\right)(\cos(k_1^h h) + \cos(k_2^h h)) \\
&- \left(\frac{4}{3} + \frac{(kh)^2}{9}\right)\cos(k_1^h h)\cos(k_2^h h) = 0.
\end{aligned} \tag{58}$$

Likewise, exact plane-wave solutions of (6) are $u(\mathbf{x}) = e^{\mathrm{i}\mathbf{k}\cdot\mathbf{x}}$, with $|\mathbf{k}| = k$.

The joint plot of $\mathbf{k}^h h$ and $\mathbf{k}h$, for $kh = 1, 2, 3$, is presented in Figure 25; it is seen that the dispersion error depends on the direction of propagation of the wave. A discrete wave-number $\mathbf{k}^h$ has to be compared with the corresponding exact wave-number which is aligned, that is, $\mathbf{k} = k\frac{\mathbf{k}^h}{\|\mathbf{k}^h\|}$: the dispersion error is $\frac{\|\mathbf{k}^h - \mathbf{k}\|}{\|\mathbf{k}^h\|} \equiv \left|1 - \frac{k}{\|\mathbf{k}^h\|}\right|$. The plot of $\frac{k}{\|\mathbf{k}^h\|}$ versus $\mathbf{k}^h h$ is given in Figure 26.

Turning to spectrum analysis, we now consider, on the domain $\Omega = (0, L) \times (0, L)$, a mesh made of n_{el} elements per direction. Taking into account the boundary conditions, there are $N = (n_{el} - 1)^2$ degrees-of-freedom. The discrete equations are analogues of (57), by invoking the change of notation $k \leftrightarrow \omega^h$ and $u_{\mathbf{A}} = \phi_{\mathbf{A}}$. The normal modes are

$$\phi_{\mathbf{A}} = C\sin(\omega_1 h A_1)\sin(\omega_2 h A_2), \qquad \forall A_1, A_2 = 0, \ldots, n_{el}, \tag{59}$$

with $1 \leq \omega_1 L/\pi, \omega_2 L/\pi \leq n_{el} - 1$. These are the interpolants of the exact normal modes $\phi_{\mathbf{x}} = C\sin(\omega_1 x_1)\sin(\omega_2 x_2)$. It can be noticed that (59) can be expanded as

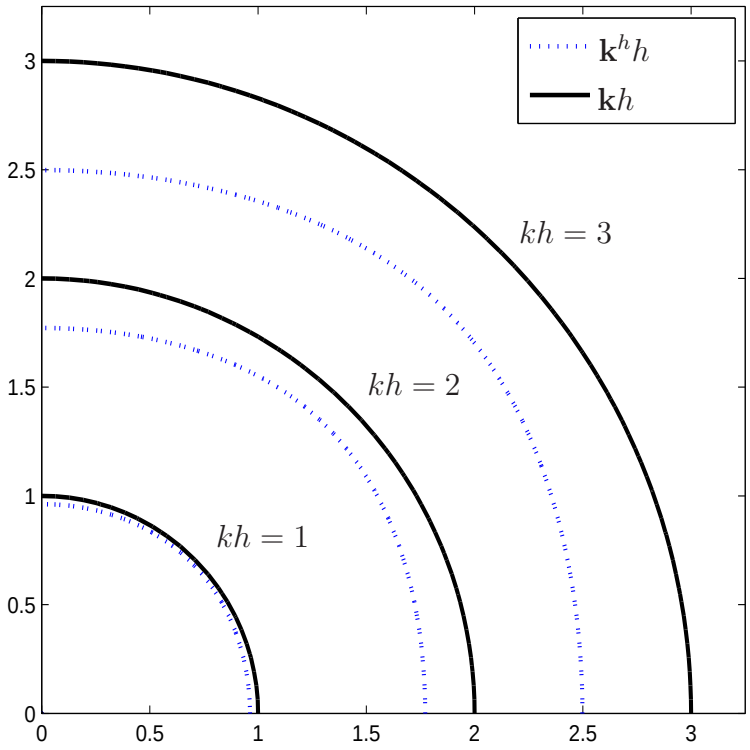

Fig. 25. Numerical wave-number $\mathbf{k}^h$ and exact wave-number $\mathbf{k}$ for $k = 1, 2, 3$ in two-dimensions, for bilinear element approximation.

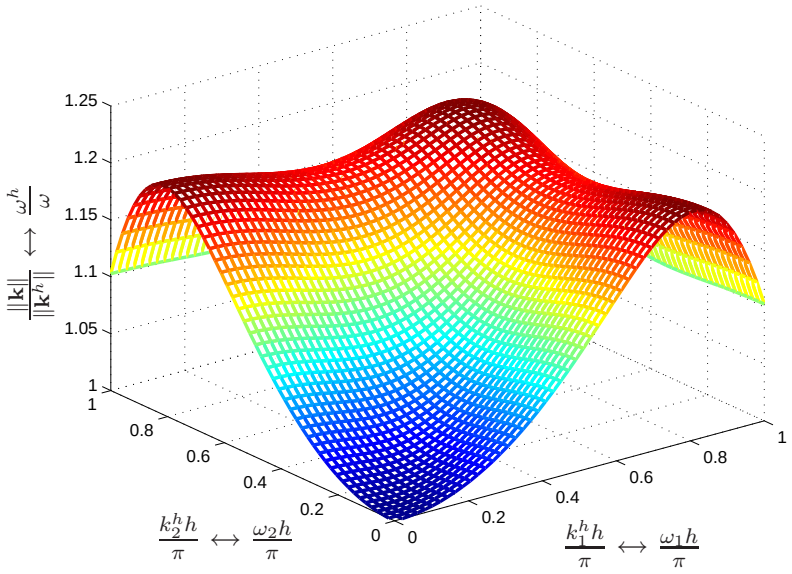

Fig. 26. Unified dispersion and spectrum analysis in two-dimensions, for bilinear approximation.

a sum of four plane waves

$$\phi_{\mathbf{A}} = C\left(e^{\mathrm{i}h(\omega_1,\omega_2)\cdot\mathbf{A}} + e^{\mathrm{i}h(-\omega_1,-\omega_2)\cdot\mathbf{A}} - e^{\mathrm{i}h(-\omega_1,\omega_2)\cdot\mathbf{A}} - e^{\mathrm{i}h(\omega_1,-\omega_2)\cdot\mathbf{A}}\right), \tag{60}$$

for $\mathbf{A} = (A_1, A_2)$, and $A_1, A_2 = 0, \ldots, n_{el}$. Therefore, we are exactly in the situation of the previous dispersion analysis. Fixing ω_1 and ω_2 by changing notation $k_1^h \leftrightarrow \omega_1$, $k_2^h \leftrightarrow \omega_2$, and using (58), the discrete frequency is obtained from the relation

$$\begin{aligned}&\left(\frac{8}{3} - \frac{4}{9}(\omega^h h)^2\right) - \left(\frac{2}{3} + \frac{2}{9}(\omega^h h)^2\right)(\cos(\omega_1 h) + \cos(\omega_2 h)) \\ &- \left(\frac{4}{3} + \frac{(\omega^h h)^2}{9}\right)\cos(\omega_1 h)\cos(\omega_2 h) = 0.\end{aligned} \tag{61}$$

The corresponding exact frequency is $\omega = \sqrt{\omega_1^2 + \omega_2^2}$. Unifying dispersion and spectrum analysis, the discrete-to-exact frequency ratio $\frac{\omega^h}{\omega}$ versus $\omega_1 h,\ \omega_2 h$ is shown in Figure 26.

When spectrum analysis is carried out numerically, as in [7] for example, the computed frequencies ω^h and the exact ones ω are sorted independently, by increasing magnitude, and then associated. In one-dimension this produces the correct association of vibrating modes, and results in the same ω^h/ω plot obtained analytically (see Remark 1). In multi-dimensions, however, this numerical procedure does not guarantee the correct association of modes and indeed the ω^h/ω numerically calculated differs from the analytical one. However, it is shown in Figure 27 that the two results are qualitatively similar, the numerical plot presenting less oscillations but still revealing the correct order of magnitude of the error.

6 Numerical results

In this section, we present several numerical experiments supporting the analytical results previously obtained. In particular, for both k- and p-methods, we examine the approximation of frequencies and modes for structural dynamics problems, while, for wave propagation, we study the approximation of response spectra, as well as determine solutions of a 1D boundary value problem proposed in the literature (cf. [22]).

We finally show preliminary results on the effects of under integrating NURBS discretizations, compared with analogous FEM results.

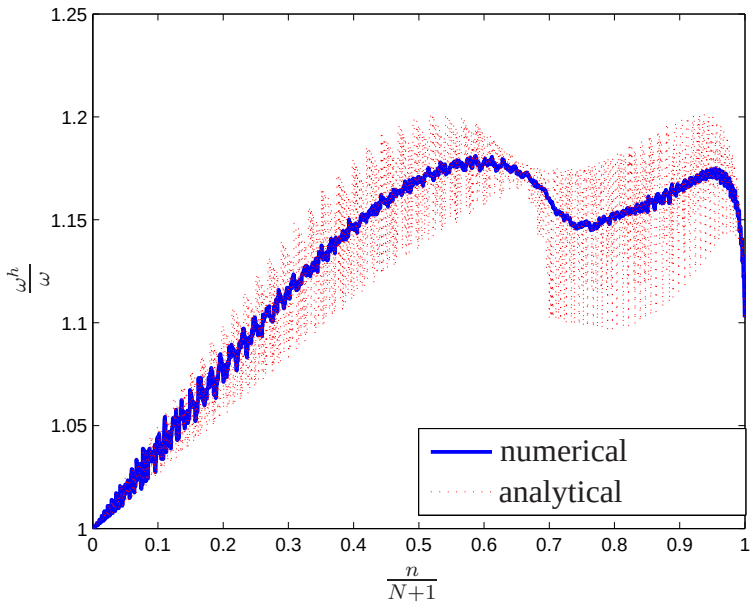

Fig. 27. Plots of $\frac{\omega^h}{\omega}$ obtained analytically (by making first the correct association of modes, and then ordering them such that ω is increasing) and numerically (by first ordering independently the frequencies and then associating them); $N = 50$.

6.1 Structural vibrations

We present results of frequency calculations for 1D and 2D cases, and we study the approximation of eigenmodes in 1D.

6.1.1 1D problems

We present the results of some numerical tests performed using the k-method (i.e., NURBS) and p-method (i.e., FEM) on a 1D vibration problem (i.e., the problem of the longitudinal vibrations of an elastic rod). In the previous section, this has been pointed out to be equivalent to the classical time-harmonic dispersion analysis for 1D wave propagation, by the duality principle.

Before comparing NURBS and FEM results, we briefly remark that the following plots for NURBS are obtained using a nonlinear parameterization (as described in Section 3.3) in order to avoid so-called "outlier frequencies". These are spurious frequencies (or discrete optical branches) that show up when a linear parameterization is employed. For a more detailed discussion on the appearance of outliers and how to eliminate them, the reader is referred to Section 4.3 and to [7].

Figure 28 shows a comparison of k- and p-method numerical spectra for $p = 1, ..., 4$ (we recall that for $p = 1$ the two methods coincide). Here, the superiority of the isogeometric approach is evident, as one can see that optical branches of spectra

diverge with p for classical C^0 finite elements. This negative result shows that even higher-order finite elements have no approximability for higher modes in vibration analysis, and possibly explains the fragility of higher-order finite element methods in nonlinear and dynamic applications, in which higher modes necessarily participate.

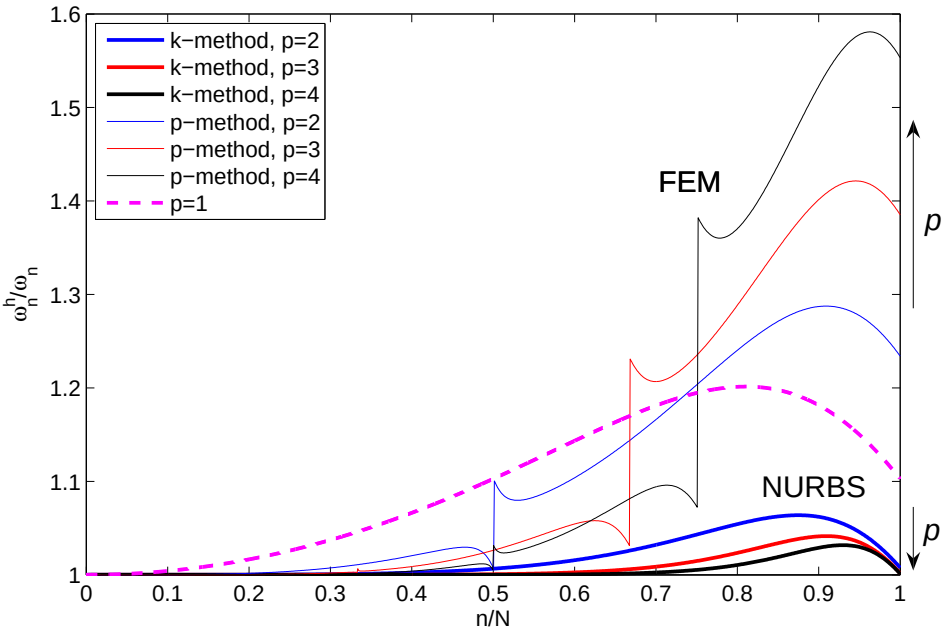

Fig. 28. Comparison of k-method and p-method numerical spectra.

Finally, following [22], we study the approximation of eigenmodes by k- and p-methods. In [22], Thompson and Pinsky consider the 1D eigenproblem corresponding to the vibration of a fixed-fixed rod of unit length, discretized with 21 degrees-of-freedom (19 after imposing the boundary conditions) and with quadratic interpolations; in particular, they study the finite element approximation of the 18^{th} mode. In order to compare the modal approximation properties of k- and p-methods, we compute eigenmodes 6, 9, 12, 15 and 18 for this same problem and we compare the numerical modes with the analytical ones, namely,

$$\phi_j(x) = \sin(j\pi x), \tag{62}$$

where j is the mode number. Figures 29-33 present the comparisons and clearly demonstrate the better performance of the k-method in approximating eigenmodes, especially ones corresponding to higher frequencies.

6.1.2 2D problems

We conclude with a comparison of k- and p-method numerical spectra for a 2D problem (i.e., the problem of the transverse vibration of a membrane).

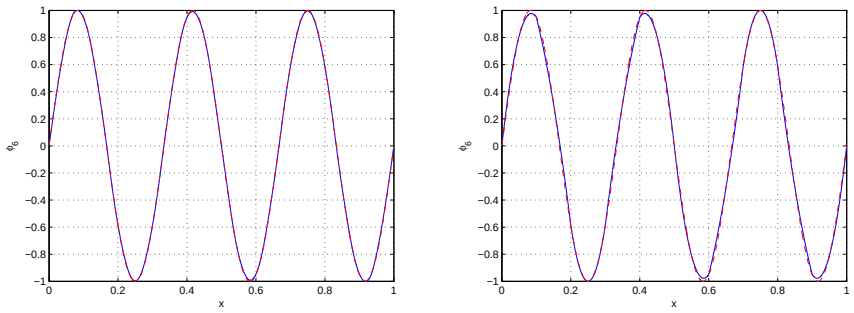

Fig. 29. Exact (red dotted line) versus numerical (blue solid line) 6^{th} eigenmode. Left: k-method approximation; right: p-method approximation.

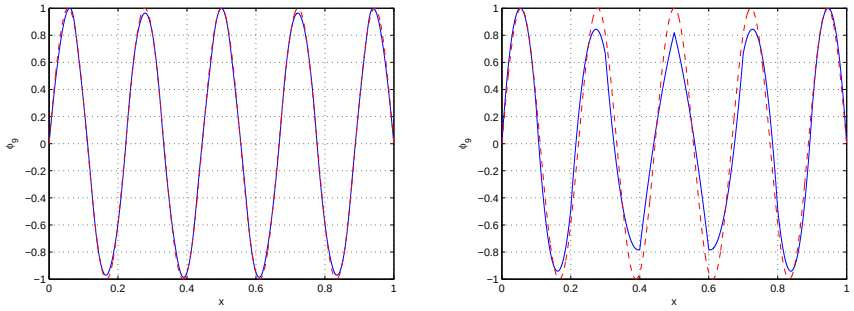

Fig. 30. Exact (red dotted line) versus numerical (blue solid line) 9^{th} eigenmode. Left: k-method approximation; right: p-method approximation.

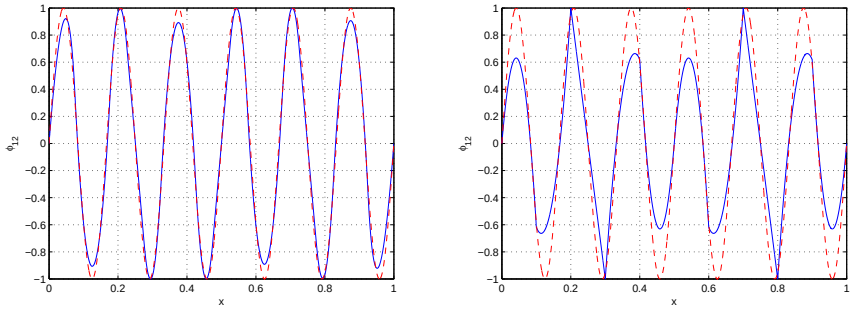

Fig. 31. Exact (red dotted line) versus numerical (blue solid line) 12^{th} eigenmode. Left: k-method approximation; right: p-method approximation.

As discussed in Section 5, we follow [7] and represent 2D spectra obtained numerically as we did for 1D, that is, the abscissae are the normalized numbers of modes sorted from the smallest to the highest frequencies. Figure 34 reports the numerical spectra obtained using 70x70 degrees-of-freedom. The results exhibit similarities to the 1D case and the superiority of the isogeometric approach is also clear. Again, for higher frequencies, finite element spectra seem to diverge with p.

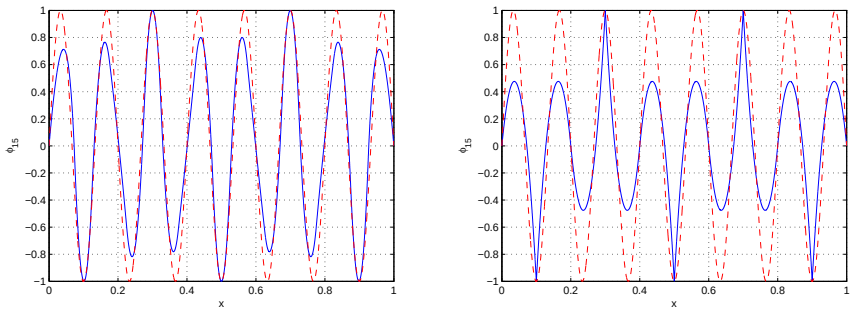

Fig. 32. Exact (red dotted line) versus numerical (blue solid line) 15^{th} eigenmode. Left: k-method approximation; right: p-method approximation.

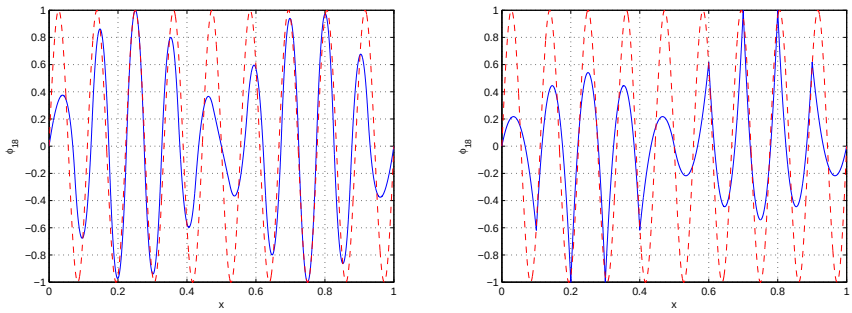

Fig. 33. Exact (red dotted line) versus numerical (blue solid line) 18^{th} eigenmode. Left: k-method approximation; right: p-method approximation.

6.2 Wave propagation

The aim of this section is to compare NURBS elements and classical finite elements on wave propagation problems. In particular, we study the problem of an elastic rod originally proposed in [22] and we use the k- and the p-methods to compute the numerical frequency response spectra and to solve a boundary value problem. We note in passing that Figure 28 can also be interpreted as representing dispersion error in wave propagation according to the duality principle. As before we need to make the interchange $\omega^h/\omega \leftrightarrow k/k^h$ and $k^h h \leftrightarrow \omega h$. In the following, all the numerical tests are carried out using quadratic and cubic elements.

6.2.1 Frequency response spectra

Following [22], we start from the governing equation of the steady-state vibration problem for a rod of length L

$$\frac{\mathrm{d}^2\phi}{\mathrm{d}x^2} + k\phi = 0, \tag{63}$$

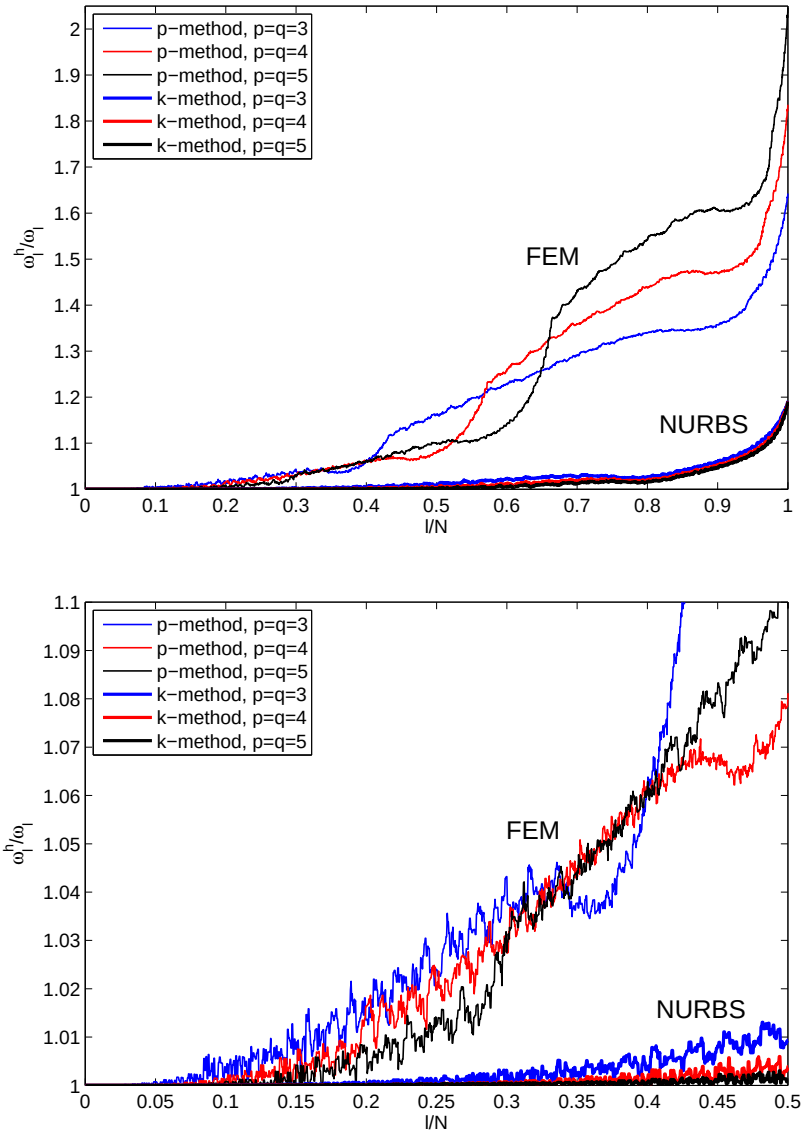

Fig. 34. Comparison of 2D k-method and p-method numerical spectra. Top: entire spectrum. Bottom: detail of the first half of the spectrum.

with boundary conditions

$$\phi(0) = \bar{\phi}, \quad \phi(L) = 0. \tag{64}$$

The solution to problem (63)-(64) can be written as

$$\phi(x,k) = \bar{\phi}\frac{\sin(k(L-x))}{\sin(kL)}. \tag{65}$$

We denote by $\phi^h(x,k)$ the numerical solution for the discrete methods. Now, the

dispersive and attenuation characteristics can be investigated using the frequency response function for both k- and p-methods, that is, we compare for each discrete method the values of $\log_{10}(R(x,k))$ with the corresponding exact values, where

$$R(x,k^h) = \phi^h(x,k)/\bar{\phi}. \tag{66}$$

Figures 35 and 36 show the response spectra obtained for $p = 2$ and $p = 3$ at $x = L/10$, $L/2$, and $9L/10$. In all cases, the better approximation properties of the k-method are evident, as well as the very poor performance of the p-method within stopping bands (see Figure 18 and [22] regarding cubic p-method stopping bands).

6.2.2 Boundary value problem

We solve the 1D boundary value problem for different choices of the wave-number k (taking, e.g., $\bar{\phi} = 1$ and $L = 1$). In order to have meshes with elements of the same length ($h = 1/10$) independent of the approximation order, we use 21 degrees-of-freedom for quadratics and 31 for cubics.

In Figures 37 and 38, we present the boundary value problem results for both k- and p-methods solved with $k = 10$, 20, 30, and 33 (i.e., within the p-method stopping band) for quadratic approximations, and with $k = 10$, 20, 30, 31.5 (i.e., within the 1^{st} p-method stopping band), 40, 50, and 71 (i.e., within the 2^{nd} stopping band, see Figure 18) for cubic approximations. In the case of NURBS, no evident attenuation is observed within the 1^{st} stopping band, which is very narrow and has a very small imaginary part (see Figure 18). The phase opposition observed in the p-method for $k = 31.5$ is indeed due to the fact that at $k = 10\pi < 31.5$ an exact resonance peak occurs, which is approximated by the p-method slightly after $k = 31.5$. For the sake of completeness, Figure 39 shows in more detail what happens around an exact resonance. We wish to emphasize that these resonance peaks do not appear in the frequency response spectra of Figure 36, since the corresponding (exact and discrete) eigenmodes vanish at $x = L/10$, $L/2$, and $9L/10$.

These figures confirm the superiority of the k-method in wave propagation. It is noted that the p-method stopping bands result in spurious attenuation of waves, due to imaginary parts of discrete wave-numbers.

6.3 Under integration

We perform an initiatory investigation of approximate integration, an issue which is of considerable importance in practical analysis.

For p- method finite elements, numerical quadrature seems to be fairly well understood. If we assume the simple case of integrating polynomials over elements, the

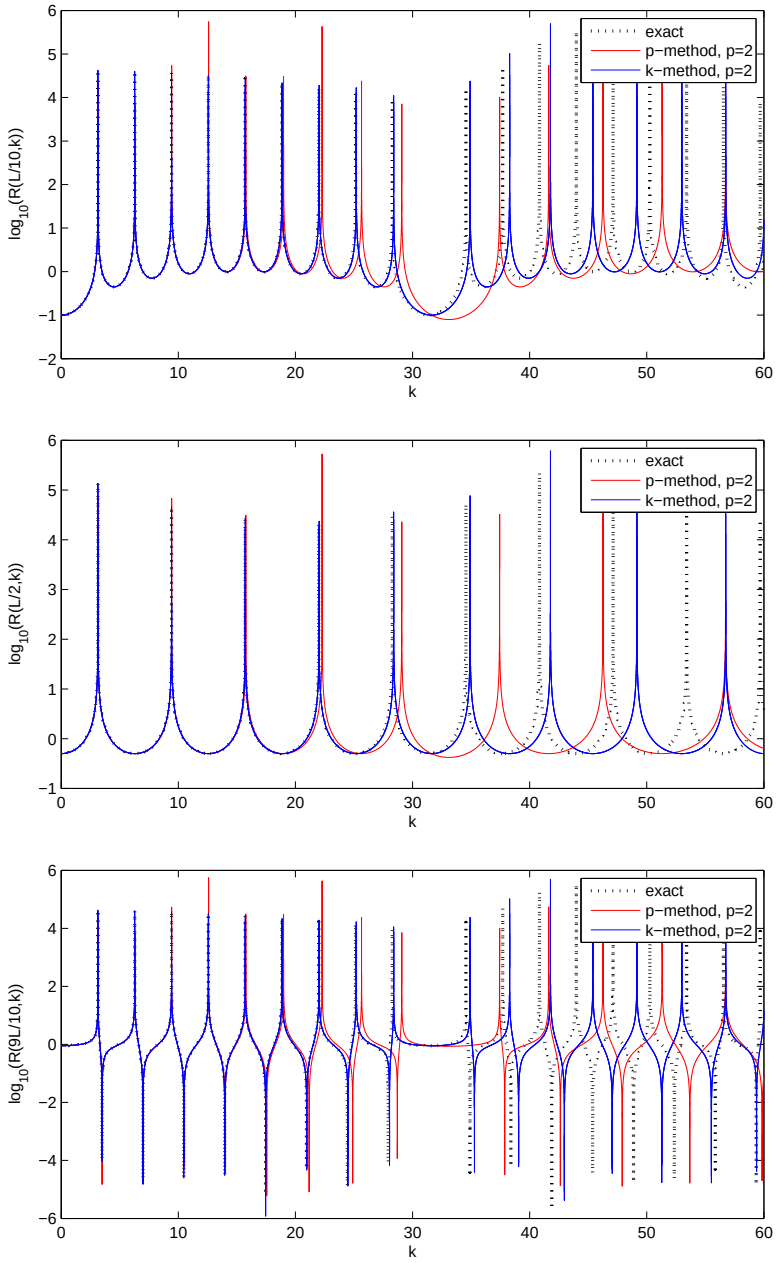

Fig. 35. Frequency response spectra for $p = 2$ computed at $L/10$ (top), $L/2$ (middle), and $9L/10$ (bottom).

Gauss rules are optimal in one dimension, and often utilized for tensor-product-based multidimensional elements. For NURBS and B-splines, the situation does not seem to be very well understood, even in one dimension. The problem here is that reduced continuity exists at *all* knots. Even in the case of the k-method, the continuity across knots internal to a patch is $C^k = C^{p-1}$. To form stiffness matrices, we need to differentiate, and form products of derivatives, resulting in polynomials of order $2(p-1)$ and continuity C^{p-2}. It seems what is required for B-splines and NURBS are rules that account for the degree of smoothness across knots, and the

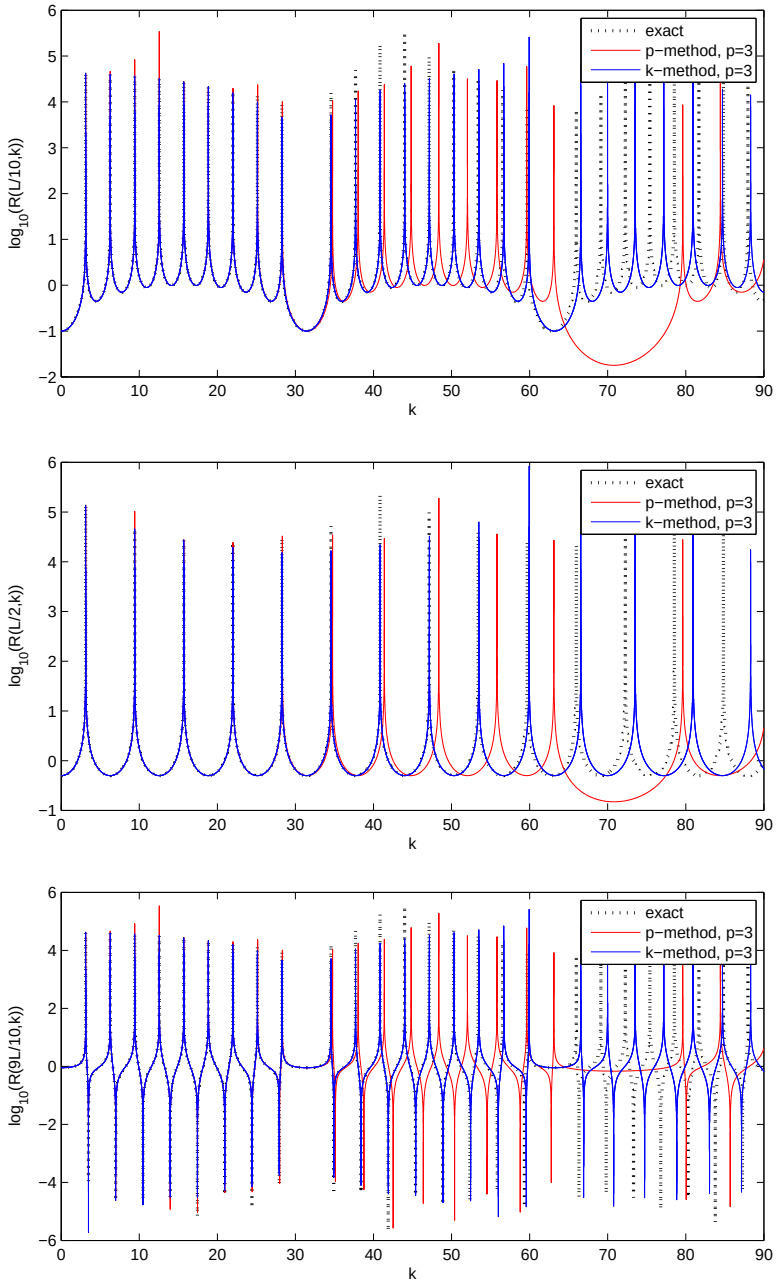

Fig. 36. Frequency response spectra for $p = 3$ computed at $L/10$ (top), $L/2$ (middle), and $9L/10$ (bottom).

precise basis on each patch. An investigation into this is beyond the scope of this paper. We shall use an approach here that is simple and effective, but very inefficient, at least for the k-method. It makes use of the observation that between knots, NURBS and B-splines are C^∞ and so are their derivatives. Consequently, Gauss rules are effective. However, this amounts to overkill compared with the usual C^0 finite elements because their basis functions are C^∞ across internal nodes (i.e., knots). Thus, for example, in one dimension, for equal order k- and p-methods one

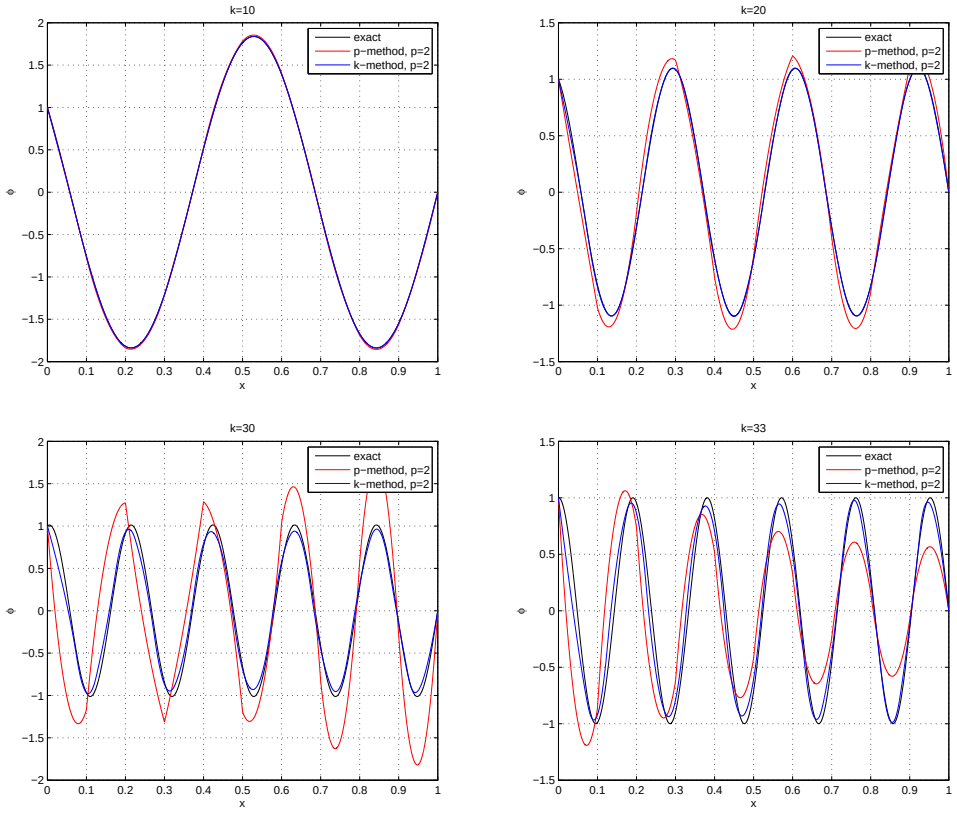

Fig. 37. Boundary value problem solution for $p = 2$ computed with $k = 10$ (top-left), $k = 20$ (top-right), $k = 30$ (bottom-left), and $k = 33$ (bottom-right, within the p-method stopping band).

would be using p times as many points for the k-method as the p-method, because for the k-method the rule needs to be used in each knot interval, whereas for the p-method it only needs to be used for each element, consisting of p consecutive knot intervals. Nevertheless, this will be the basis of this initiatory comparison. It should be emphasized that this means that many more points are being used in the k-method than for the p-method. However, conclusions drawn should be viewed as preliminary, at least, until optimal rules are developed for NURBS and B-splines.

6.3.1 1D spectrum approximation

We start by considering 1D problems and pointing out that $p + 1$ Gauss points are needed in order to exactly integrate both mass and stiffness matrices obtained from degree p basis functions (in the following, we will refer to this case as "full integration"). Instead, using p Gauss points (i.e., "under integrating" using one fewer Gauss point), the mass matrix is under integrated while the stiffness is still exactly integrated. Using less than p Gauss points, we under integrate both mass and stiffness. We remark that all the results presented prior to this section have been obtained using full integration.

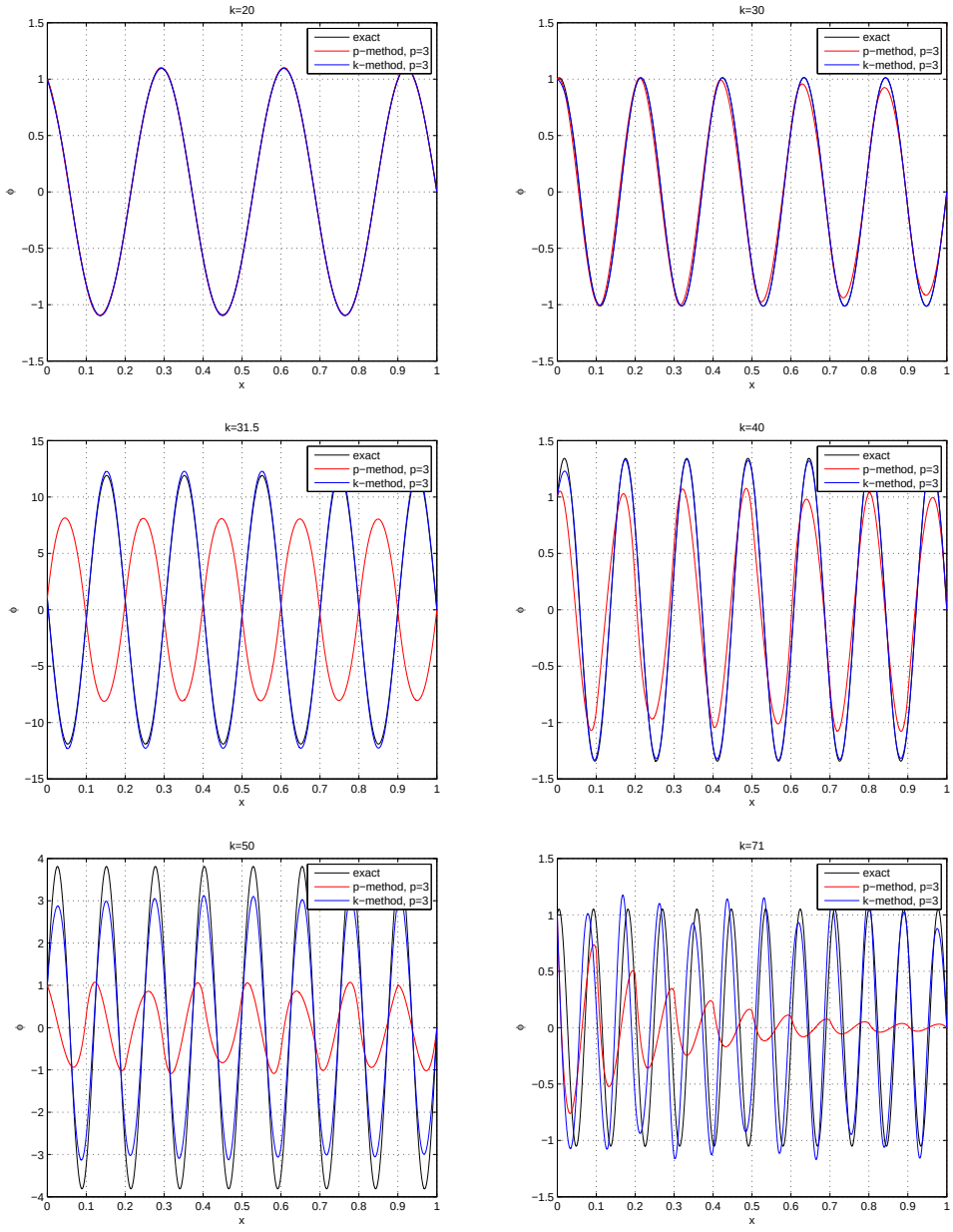

Fig. 38. Boundary value problem solution for $p = 3$ computed with $k = 20$ (top-left), $k = 30$ (top-right), $k = 31.5$ (middle-left, within the 1^{st} p-method stopping band), $k = 40$ (middle-right), $k = 50$ (bottom-left), and $k = 71$ (bottom-right, within the 2^{nd} stopping band).

We first study what happens when under integrating p-method matrices in spectrum analysis. Indeed, in this case, we can only under integrate by 1 Gauss point, otherwise stability is lost (i.e., the stiffness matrix becomes singular). Moreover, the under integrated results are even worse than the fully integrated ones in that, for *fixed* p, the highest frequency error *diverges* as the mesh is refined. See Figures 40 and 41 in which 1000 control points were used.

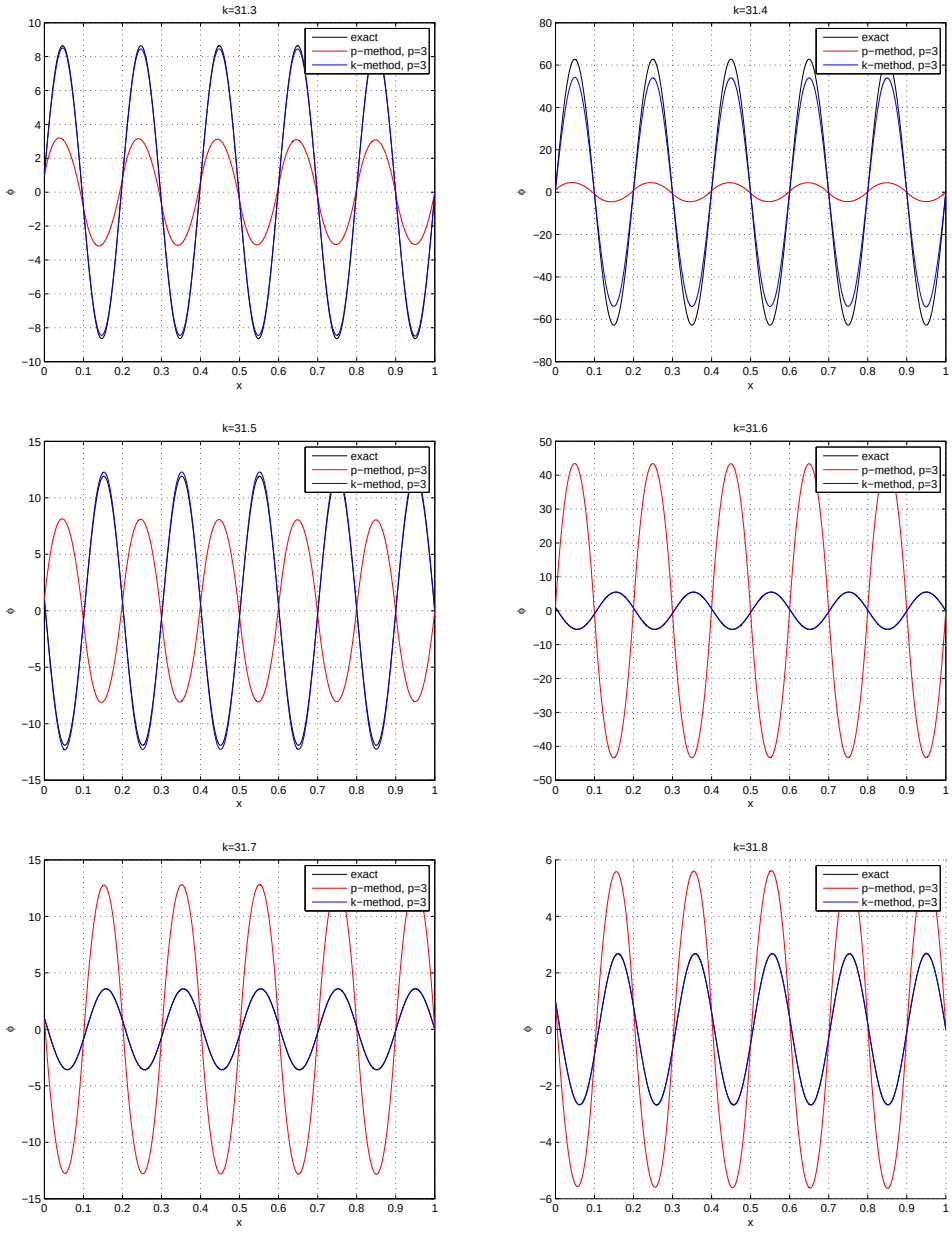

Fig. 39. Boundary value problem solution for $p = 3$ computed with $k = 31.3$ (top-left), $k = 31.4$ (top-right), $k = 31.5$ (middle-left), $k = 31.6$ (middle-right), $k = 31.7$ (bottom-left), and $k = 31.8$ (bottom-right), illustrating what happens around the exact resonance peak occurring at $k = 10\pi$.

Better results are obtained under integrating k-method matrices by 1 Gauss point, as shown in Figure 42. Moreover, it is interesting to observe that acceptable results are often obtained under integrating k-method matrices by even more than 1 Gauss points, as shown in Figure 43. For $p \geq 2$ stability is always lost when using just 1 Gauss point, so in the tests we integrated with a minimum of 2 Gauss points.

Figure 44 shows the number of Gauss points needed for full quadrature, and the

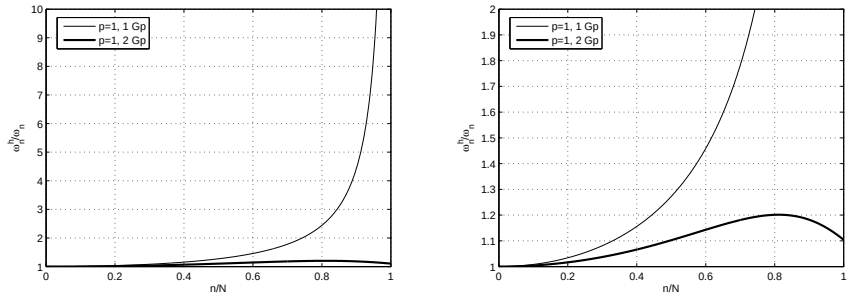

Fig. 40. 1D numerical spectra for linear basis functions obtained with full integration compared with spectra under integrated by 1 Gauss point (plotted at two different scales).

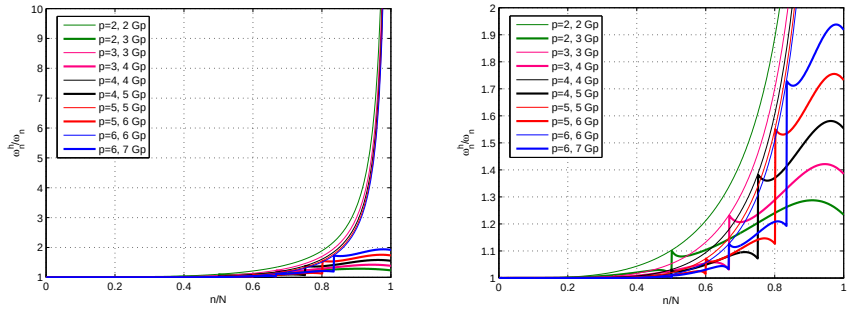

Fig. 41. 1D p-method numerical spectra obtained with full integration compared with spectra under integrated by 1 Gauss point (plotted at two different scales).

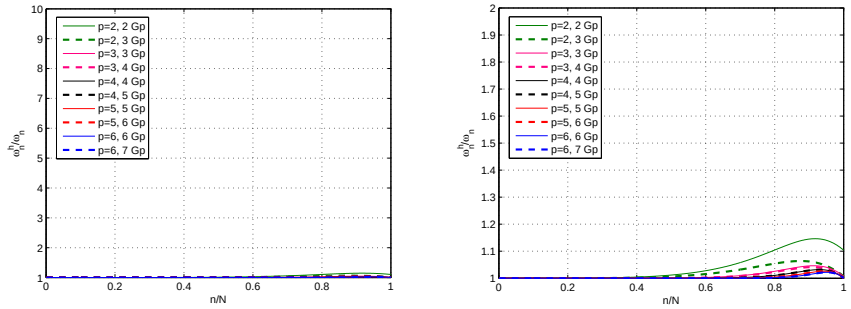

Fig. 42. 1D k-method numerical spectra obtained with full integration compared with spectra under integrated by 1 Gauss point (plotted at two different scales).

minimum necessary for stability. Perhaps the most interesting information presented in Figure 44 is the minimum number of Gauss points needed to get "acceptable" results. We remark that the "acceptable" level is here defined by a subjective evaluation of the spectrum approximation properties given on the basis of the results reported in Figure 43 and some other numerical calculations. It is interesting to note that the number of Gauss points needed to reach acceptable results for the k-method is described by the expression $round\_up(p/2) + 1$ (where $round\_up(\cdot)$ is the round-toward-infinity function). Asymptotically, the slope of this function is $1/2$, half that for full quadrature.

A rigorous mathematical explanation of the effects of under integration on p- and

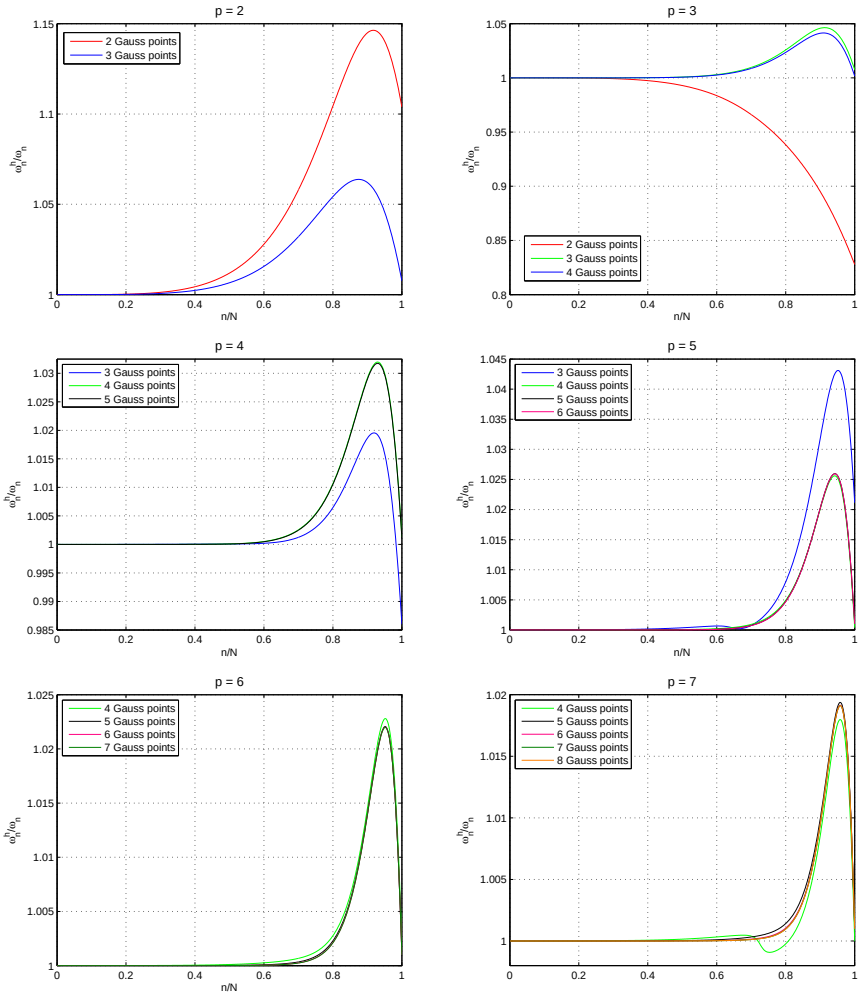

Fig. 43. 1D k-method numerical spectra obtained with full integration compared with under integrated ones, for different choices of the order p.

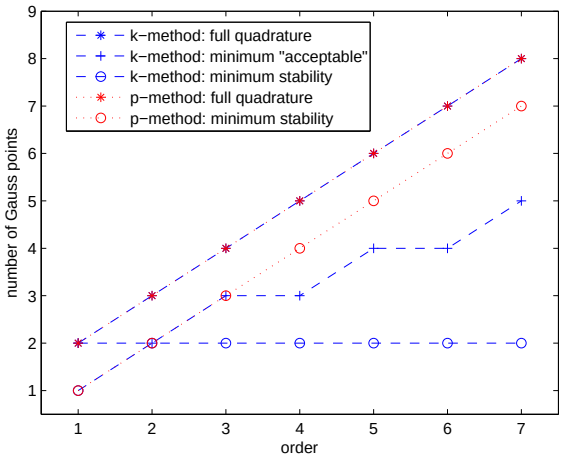

Fig. 44. Quadrature limits for p- and k-methods.

k-methods is an open question. Furthermore, it is important to develop new and more efficient quadrature rules for the k-method so that its full potential can be reached. The stability of the k-method with reduced quadrature suggests to us that this should be possible.

7 Conclusions

We compared the approximation properties of standard C^0 continuous finite elements with NURBS on problems of structural vibrations and wave propagation. The basis of the comparison is the same number of degrees of freedom, equivalently, the bandwith of the matrix system. We found that the higher-modes of classical p-method finite elements, represented by so-called "optical branches" of the frequency spectrum, have no approximability whatsoever (not surprising) and that the errors in frequency diverge with p (very surprising). The behavior of NURBS is much better. The entire spectrum converges with p. This suggests to us that NURBS present the possibility of higher order accuracy *and* robustness. Heretofore, within the finite element method, these attributes have been mutually exclusive. We also articulated a "duality principle" which provides precise correspondence between spectrum analysis in structural dynamics and dispersion analysis in wave propagation. Lastly, we performed an initial study of reduced quadrature, being fully aware that optimal quadrature rules are not yet available for NURBS. Nevertheless, the results suggest that reducing the number of quadrature points for NURBS by a significant amount is feasible. We hope to pursue this issue in future works.

Acknowledgments

T.J.R. Hughes expresses his appreciation for support provided by the Office of Naval Research under Contract No. N00014-03-0263, Dr. Luise Couchman, contract monitor. A. Reali and G. Sangalli were partially supported by the J.T. Oden Faculty Fellowship Research Program at the ICES. A. Reali was partially supported by Regione Lombardia through the INGENIO research program No. A0000800, as well as by the Ministero dell'Università e della Ricerca (MiUR) through the PRIN 2006 research program No. 2006083795. G. Sangalli was partially supported by the Ministero dell'Università e della Ricerca (MiUR) through the PRIN 2006 research program No. 2006013187. This support is gratefully acknowledged.

References

[1] M. Ainsworth. Discrete dispersion relation for hp-version finite element approximation at high wave-number. *SIAM Journal on Numerical Analysis*, **42**, 553–575, 2004.

[2] Y. Bazilevs, L. Beirão de Veiga, J.A. Cottrell, T.J.R. Hughes, G. Sangalli. Isogeometric analysis: approximation, stability and error estimates for h-refined meshes. *Mathematical Models and Methods in Applied Sciences*, **16**, 1–60, 2006.

[3] L. Brillouin. *Wave Propagation in Periodic Structures*. Dover Publications, 1953.

[4] A.K. Chopra. *Dynamics of Structures. Theory and Applications to Earthquake Engineering, Second Edition*. Prentice-Hall, 2001.

[5] R.W. Clough, J. Penzien. *Dynamics of Structures*. McGraw-Hill, 1993.

[6] E. Cohen, R.F. Riesenfeld, G. Elber. *Geometric Modeling with Splines*. A.K. Peters, 2001.

[7] J.A. Cottrell, A. Reali, Y. Bazilevs, T.J.R. Hughes. Isogeometric analysis of structural vibrations. *Computer Methods in Applied Mechanics and Engineering*, **195**, 5257–5296, 2006.

[8] J.A. Cottrell, T.J.R. Hughes, A. Reali. Studies of Refinement and Continuity in Isogeometric Structural Analysis. *Computer Methods in Applied Mechanics and Engineering*, **196**, 4160–4183, 2007.

[9] A. Deraemaeker, I. Babuška, and P. Bouillard. Dispersion and pollution of the fem solution for the Helmholtz equation in one, two and three dimensions. *International Journal for Numerical Methods in Engineering*, **46**, 472–499, 1999.

[10] G.E. Farin. *NURBS curves and surfaces: from projective geometry to practical use*. A.K. Peters, 1995.

[11] H. Gomez, V. Calo, Y. Bazilevs, T.J.R. Hughes. Isogeometric analysis of the Cahn-Hilliard phase field model. In preparation, 2007.

[12] I. Harari and T.J.R. Hughes. Finite element methods for the Helmholtz equation in an exterior domain: model problems. *Computer Methods in Applied Mechanics and Engineering*, **87**, 59–96, 1991.

[13] I. Harari and T.J.R. Hughes. Galerkin/least-squares finite element methods for the reduced wave equation with nonreflecting boundary conditions in unbounded domains. *Computer Methods in Applied Mechanics and Engineering*, **98**, 411–454, 1992.

[14] T.J.R. Hughes. *The Finite Element Method: Linear Static and Dynamic Finite Element Analysis*. Dover Publications, 2000.

[15] T.J.R. Hughes, J.A. Cottrell, Y. Bazilevs. Isogeometric analysis: CAD, finite elements, NURBS, exact geometry, and mesh refinement. *Computer Methods in Applied Mechanics and Engineering*, **194**, 4135–4195, 2005.

[16] F. Ihlenburg and I. Babuška. Dispersion analysis and error estimation of Galerkin finite element methods for the Helmholtz equation. *International Journal for Numerical Methods in Engineering*, **38**, 3745–3774, 1995.

[17] W.Y. Kwok, R.D. Moser, J. Jiménez . A Critical Evaluation of the Resolution Properties of B-Spline and Compact Finite Difference Methods. *Journal of Computational Physics*, **174**, 510–551, 2001.

[18] L. Piegl and W. Tiller. *The NURBS Book, 2nd Edition*. Springer-Verlag, 1997.

[19] A. Reali. An isogeometric analysis approach for the study of structural vibrations. *Journal of Earthquake Engineering*, **10**, s.i. 1, 1–30, 2006.

[20] R.D. Richtmyer, K.W. Morton. *Difference Methods for Initial-value Problems. Second Edition*. John Wiley & Sons, 1967.

[21] D.F. Rogers. *An Introduction to NURBS With Historical Perspective*. Academic Press, 2001.

[22] L.L. Thompson and P.M. Pinsky. Complex wavenumber Fourier analysis of the p-version finite element method. *Computational Mechanics*, **13** 255–275, 1994.

[23] L.L. Thompson, P.M. Pinsky. Acoustics. (E. Stein, R. De Borst, T.J.R. Hughes eds.) *Encyclopedia of Computational Mechanics*, Wiley InterScience, Vol. 2, Chap. 22, 2004.

[24] L.L. Thompson. A review of finite element methods for time-harmonic acoustics. *Journal of the Acoustical Society of America*, **119**, 1315–1330, 2006.